

# Smart nanoparticles as advanced anti-Akt kinase delivery systems for pancreatic cancer therapy

Juan Gonzalez-Valdivieso<sup>1</sup>, Andres Garcia-Sampedro<sup>2</sup>, Andrew R. Hall<sup>2,3</sup>, Alessandra Girotti<sup>4</sup>, F. Javier Arias<sup>1</sup>, Stephen P. Pereira<sup>2</sup> and Pilar Acedo<sup>2\*</sup>

<sup>1</sup>Smart Biodevices for NanoMed Group, University of Valladolid, Paseo Belén, 47011, Valladolid, Spain

<sup>2</sup>Institute for Liver and Digestive Health, Royal Free Hospital, University College London, Pond Street, NW3 2QG, London, United Kingdom

<sup>3</sup>Sheila Sherlock Liver Centre, Royal Free London NHS Foundation Trust, London, United Kingdom

<sup>4</sup>BIOFORGE (Group for Advanced Materials and Nanobiotechnology), CIBER-BBN, University of Valladolid, Paseo Belén, 47011, Valladolid, Spain

\*Corresponding author: p.nunez@ucl.ac.uk

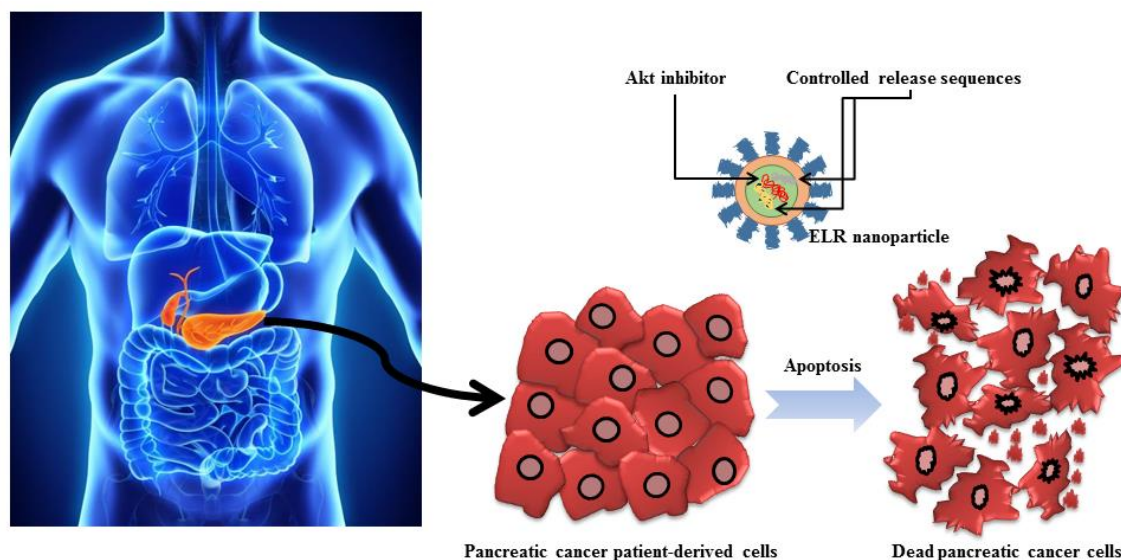
## **Abstract:**

Pancreatic cancer is one of the deadliest cancers partly due to late diagnosis, poor drug delivery to the target site and acquired resistance to therapy. Therefore, more effective therapies are urgently needed to improve the outcome of patients. In this work, we have tested self-assembling genetically engineered polymeric nanoparticles formed by elastin-like recombinamers (ELRs), carrying a small peptide inhibitor of the protein kinase Akt, in both PANC-1 and pancreatic cancer patient-derived cells (PDX models). Nanoparticle cell uptake was measured by flow cytometry and subcellular localisation was determined by confocal microscopy, which showed a lysosomal localisation of these nanoparticles. Furthermore, metabolic activity and cell viability were significantly reduced after incubation with nanoparticles carrying the Akt inhibitor in a time- and dose-dependent fashion. Self-assembling 73 nm size nanoparticles inhibited phosphorylation and consequent activation of Akt protein, blocked the NF- $\kappa$ B signalling pathway and

triggered caspase 3-mediated apoptosis. Furthermore, *in vivo* assays showed that ELR-based nanoparticles were suitable devices for drug delivery purposes with long circulating time and minimum toxicity. Hence, the use of these smart nanoparticles could lead to the development of more effective pancreatic cancer treatment options based on the inhibition of Akt.

**Keywords:** nanoparticle; drug delivery; elastin-like recombinamer; Akt; pancreatic cancer

### **Graphical abstract:**



Self-assembling nanoparticles carrying an Akt inhibitor are an accurate drug delivery system as validated in pancreatic cancer patient-derived models and a promising treatment strategy for multimodal therapy in combination with chemotherapy.

### **1. Introduction:**

Pancreatic ductal adenocarcinoma (PDAC) remains one of the deadliest forms of cancer despite the different treatments developed during the last years [1-3]. Different factors are associated with its late diagnosis, poor prognosis and low success of treatment options

available for this disease, such as the difficulty to reach the tumour site, damage to healthy tissues or the ability of pancreatic cancer cells to acquire resistance to therapeutic drugs [4-6]. Therefore, novel therapeutic strategies are urgently needed to achieve higher treatment efficacy, minimising disease relapse and undesired effects on healthy tissues [6-11]. Biomaterials have become one of the most promising therapeutic approaches for drug delivery purposes, aiming at achieving a more specific and controlled action by only affecting specific cells and overcoming the poor accumulation of current drugs in the desmoplastic pancreatic tumours [12].

Among novel biomaterials, elastin-like recombinamers (ELRs) stand out due to their multiple advantages, such as their biocompatibility, biodegradability, and stimuli responsive behaviour. ELRs are polymeric biomaterials composed by the repetition of the VPGXG pentapeptide found in the sequence of natural elastin, where X represents any amino acid except proline [13]. ELRs are created by genetic engineering techniques taking advantage of DNA recombinant technology, allowing us to control the amino acid sequence, which ultimately, determines the stimuli-responsive behaviour of the designed ELRs. Furthermore, a variety of bioactive sequences can be added to the polymers to regulate their interaction with different cellular components [14-15]. Elastin-based polymers are characterised by their inverse temperature transition (ITT), which determines the transition temperature ( $T_t$ ) below which, the polymeric chains remain as soluble disordered molecules in aqueous solution. However, when the temperature is increased above the  $T_t$ , the chains adopt an ordered  $\beta$ -spiral conformation resulting in their self-assembly in coacervates [16]. This whole process is completely reversible. The reversible coacervation of ELR polymers depends on multiple factors, such as amino acid composition, sequence, temperature, pH, ions or light. Due to their stimuli-

responsiveness behaviour, ELR-based polymers are promising tools for biomedical applications and especially for controlled drug delivery [17-23].

Even though novel biomaterials such as polymers, gold or mesoporous silica nanoparticles, among others, allow us to improve the biodistribution and circulating time of drugs in the bloodstream, nanoparticles (NPs) have emerged as an interesting strategy in order to achieve a controlled drug release in targeted tissues [24-26]. Moreover, NPs have been shown to avoid unspecific drug accumulation in vital organs, such as the liver or the kidneys, which allow the use of higher concentrations of chemotherapeutic agents, enhancing their efficacy [24, 27-28]. In addition, tumours are characterised by the well-known enhanced permeability and retention (EPR) effect showing leaky blood vessels and lack of effective lymphatic drainage, which enhances vascular permeability and the retention of drugs in the tumour site [29-32]. As a result of the EPR effect, when NPs enter the interstitial space they are not efficiently eliminated, and they remain retained in the tumour tissue. For all these reasons, optimal nanoparticle size is estimated to be between 10 and 100 nm [30, 33].

Specific cancerous markers, such as proteins or membrane receptors, are usually chosen to improve the selective accumulation and action of chemotherapeutic agents and to decrease the effect on non-cancerous cells due to their overexpression on cancerous cells compared to healthy tissues [34-35]. We selected the Akt kinase as our target protein for this study as Akt is overexpressed in different cancer cells including pancreatic, breast and colorectal among others [36]. Akt plays a pivotal role in cancer progression and chemoresistance, as it is involved in multiple key processes such as cell growth, proliferation or survival via different signalling pathways [37-39]. It has been shown that

pancreatic cancer cells have a higher expression of activated, phosphorylated, Akt kinase than normal pancreatic cells, in order to promote cell proliferation and to avoid apoptosis-mediated cell death. In normal cells, Akt remains inactivated and the kinase is only phosphorylated, in response to external stimuli, such as growth factors [4, 40].

The Akt protein is activated in two steps. First, the kinase suffers a conformational change triggered by lipid products of Phosphoinositide-3-kinase (PI3K) [41]. Then, Akt kinase is phosphorylated at threonine 308 and serine 473 residues. This mechanism of Akt activation is well known and different molecules have been designed to inhibit Akt phosphorylation as therapeutic approaches at the molecular level [42]. Among these molecules, a small 15 amino acid peptide inhibitor discovered by Hiromura *et al.* [43], Akt-in, appeared as an interesting and effective tool for the blockade of the Akt signalling pathway by avoiding phosphatidyl inositol triphosphate moieties binding to Akt protein and, as a consequence, prevented the activation of Akt kinase. In fact, the peptide showed *in vitro* inhibition of cell proliferation and anti-apoptotic activity and *in vivo* tumour regression [43]. Our proposed ELR nanoparticles for this work, carry the Akt inhibitor (Akt-in) in order to facilitate its entrance into the cellular cytoplasm, avoid its degradation and improve its therapeutic effect in pancreatic cancer cells.

One of the reasons for the low success rate of different clinical trials for PDAC is the wide intratumoural heterogeneity of pancreatic tumours formed by diverse cell types and lineages within the tumour. The often used *in vitro* cell cultures consisting of established cell lines are an important concern and limiting factor as cells arise from the same single clone, not fully represent the characteristic genetic heterogeneity of a tumour. For this reason, in this work, we have used two different clinically relevant pancreatic cancer

patient-derived cells, previously described as PDX185 and PDX354 cells [44-46]. Patient-derived models allow us to study novel therapeutic drugs in more physiological conditions including different cancer cell populations and cancer stem cells [47-48].

In the present work, we have studied the effect of a novel therapeutic treatment based on smart self-assembling ELR NPs for controlled and precise drug delivery of an Akt inhibitor to pancreatic cancer patient-derived cells. We determined the effect of our NPs on cellular metabolic activity and viability, cellular uptake and subcellular accumulation and their molecular mechanism of action. Although these ELRs nanoparticles were previously characterised and studied in breast and colorectal cancer cell cultures *in vitro* [49], it is the first time they have been evaluated as a novel strategy for PDAC therapy in patient-derived models as a first step towards the development of a novel therapy. Therefore, we developed an advanced nanocarrier for controlled drug delivery which could be a promising treatment for pancreatic cancer in combination with chemotherapy.

## **2. Materials and methods:**

### **2.1 Chemical reagents and cell lines**

LIVE/DEAD<sup>®</sup> Viability/Cytotoxicity Kit for mammalian cells and LysoTracker Red DND-99 were supplied by Invitrogen. Thiazolyl Blue Tetrazolium Bromide (MTT), anhydrous N,N Dimethylformamide (DMF), Dimethyl sulfoxide (DMSO), methanol, and DMEM media (Dulbecco's Modified Eagle's Medium) were purchased from Sigma-Aldrich. Foetal Bovine Serum (FBS), penicillin/streptomycin, RPMI media (Roswell Park Memorial Institute), Trypsin-EDTA and Phosphate Buffered Saline (PBS) were supplied by Gibco. NHS-Fluorescein and NHS-Cy5 were provided by Lumiprobe. Neutral Red reagent was supplied by Panreac Quimica. DePex mounting medium was

purchased from Serva. Cell lysis RIPA buffer and Bradford reagent were supplied by BIORAD. PhosSTOP® phosphatase inhibitor cocktail and COMPLETE® protease inhibitor cocktail were purchased from Roche. Primary antibodies against total Akt (#9272), p-Akt Ser473 (#9271), p-JNK (#9251), NF-κB p65 (#4764), cleaved caspase-3 Asp175 (#9661), β-actin (#3700) and GAPDH (sc-32233) were purchased from Cell Signalling and Santa Cruz Biotechnology. Goat secondary antibodies against rabbit (P0448) and mouse (P0447) were supplied by Dako. Western-Ready ECL Substrate kit was supplied by BioLegend. Isoflurane was purchased from Esteve. Harris Haematoxylin and Eosin were purchased from Leica.

Human pancreatic cancer cells PANC-1 (ATCC® CRL-1469™) were purchased from the American Type Culture Collection (ATCC). Pancreatic adenocarcinoma patient-derived xenograft models (PDXs) 354 and 185 were obtained from the Biobank of the Spanish National Cancer Research Centre (CNIO), Madrid, Spain (references B18230PDX7, B18243PDX4). Cells were isolated from these tumours and established for *in vitro* culture as described in [50].

## **2.2 ELR design, bioproduction and purification**

The ELRs used in this work were obtained as previously described [49, 51]. The construction of the final fusion genes with fully controlled chain composition and length was carried out by sequential introduction of the monomer genes by using the recursive directional ligation method (RDL). The expression vectors containing the desired ELR genes were transformed into *Escherichia coli* BLR (DE3) strain and bioproduced in a 15-L bioreactor (Applikon Biotechnology). The ELRs were purified by several cooling and heating purification cycles (Inverse Transition Cycling-ITC) and additional NaCl and

NaOH treatments were performed in order to remove endotoxins [52]. Finally, the product was dialysed against ultrapure water type I, sterilised by filtration (0.22  $\mu\text{m}$  filters Nalgene) and freeze-dried prior to storage. Sodium dodecyl sulfate polyacrylamide gel electrophoresis (SDS-PAGE) and mass spectrometry (MALDI-TOF/MS) were performed to determine the molecular weight and purity of the recombinamers. High Performance Liquid Chromatography (HPLC) and Nuclear Magnetic Resonance (NMR) were carried out by Laboratory of Instrumental Technics from University of Valladolid to verify the amino acid composition. The Endosafe-PTSTM test was used in order to measure endotoxin levels (Charles River).

### **2.3 Physicochemical characterisation**

Transition temperatures were determined by Differential Scanning Calorimetry (DSC) using a Mettler Toledo 822e with a liquid nitrogen cooler. An indium standard was used for calibration of temperature and enthalpy. ELRs samples were prepared in PBS (pH 7.4) at 50 mg/mL. 20  $\mu\text{L}$  aliquot of sample and the corresponding PBS reference were subjected first to an isothermal stage (5 min at 0°C to stabilise the temperature and state of the samples), and then heated from 0 to 60°C at 5°C/min. For enthalpy values, endothermic processes were taken as negative and exothermic processes as positive.

Particle size and  $\zeta$ -potential of the polymers were determined by Dynamic Light Scattering (DLS) using a Zetasizer Nano ZS (Malvern Instruments Ltd.) at 37°C. Samples were prepared by dissolving the ELRs in PBS (pH 7.4) or ultrapure water type I (pH 7.4) when indicated. Samples were stored overnight at 4°C in order to allow complete dissolution and filtered using a 0.45  $\mu\text{m}$  poly(vinylidene difluoride) (PVDF) syringe filter. Samples were incubated at 37°C for 30 min in order to allow self-assembling and then



introduced into polystyrene cuvettes. Then, samples were stabilised for 2 min at the desired temperature before the measurements. Autocorrelation functions were used to obtain size distribution and polydispersity index (PDI). Z-average mean (nm) and  $\zeta$ -potential (mV) were used for data analysis. Three different samples were analysed for statistical purposes.

#### **2.4 Fluorescent ELR labelling**

ELR polymers were covalently modified with NHS-Fluorescein or NHS-Cy5 by conjugation to free amines, when indicated. NHS-Fluorescein or NHS-Cy5 were dissolved in DMF at 10 mg/mL. Three equivalents of fluorophore were added to ELR polymers dissolved in DMF and incubated at 4°C for 2 hours. Finally, the polymer was dialysed against ultrapure water type I in order to discard solvent and non-conjugated fluorophore and freeze-dried prior to storage.

#### **2.5 Cell culture**

Human pancreatic cancer cells PANC-1 (ATCC<sup>®</sup> CRL-1469<sup>™</sup>) were cultured in DMEM media (Dulbecco's Modified Eagle's Medium). PDX-derived cells were cultured in RPMI media (Roswell Park Memorial Institute). Both cell culture media were supplemented with 10% Foetal Bovine Serum (FBS), 100 U/mL penicillin and 0.1 mg/mL streptomycin. Cells were grown in 75 cm<sup>2</sup> tissue culture flasks (TPP) at 37°C in 95% humidity and 5% CO<sub>2</sub> and, once 70-80% confluence was reached, they were either sub-cultured or seeded for the below described protocols. When required, cells were detached using a solution of 0.05% Trypsin-EDTA.

#### **2.6 Internalisation kinetics**

PANC-1, PDX185 and PDX354 cells ( $5 \times 10^5$  cells/well in 6-well plates) were incubated with complete media containing Cy5-labelled ELR-nanoparticles at 0.5 mg/mL for 3 or 24 hours. Cells were washed three times with PBS, trypsinised and centrifuged for 10s at 16800 xg. The supernatant was discarded, and the cell pellet was resuspended in PBS. Samples were measured in a BD LSRII flow cytometer (BD Bioscience) with a laser line at 640 nm (red) and complemented with appropriate filters. 10,000 events per sample were recorded and single cells were discriminated from doublets by pulse-processing. The FlowJo v10 software (BD Bioscience) was used to analyse and plot the acquired data.

## **2.7 Subcellular localisation**

PANC-1 cells were seeded on FluoroDish glass bottom dishes (World Precision Instruments) at a density of  $8 \times 10^3$ , and allowed to attach overnight prior to treatment. Cells were treated with fluorescein-labelled ELR nanoparticles at 0.5 mg/mL for 3 or 24 hours. After washing with PBS, cells were incubated with 75 nM LysoTracker Red DND-99 (1 mM working solution in DMSO) for 1 hour at 37°C. Fluorescence images were taken with an Olympus TIRF confocal microscope equipped with SIM scanner and an incubator to maintain the conditions constant at 37°C, 95% humidity and 5% CO<sub>2</sub>.

## **2.8 Metabolic activity**

PANC-1 ( $5 \times 10^3$  cells/well) and PDX cells ( $1 \times 10^4$  cells/well) were seeded onto 96-well plates and treated with three different concentrations of ELR nanoparticles (0.25 mg/mL, 0.5 mg/mL and 1 mg/mL) for 3 and 24 hours. Following treatment, MTT assay was performed according to manufacturer's instructions. Briefly, a MTT stock solution (0.5 mg/mL) was diluted in complete media and filtered using a 0.45 µm PVDF syringe filter. 100 µL/well of MTT solution were added and samples were incubated for 1 hour in the

dark. After that, media was removed and 100  $\mu\text{L}$ /well of DMSO were added to dissolve MTT crystals. Absorbance was measured at 562 nm using an Infinite M200 PRO microplate reader (Tecan Group Ltd.). Additionally, images of cultures were taken with an EVOS™ Digital Colour Fluorescence Microscope (Fisher Scientific). Three independent experiments, each in triplicate, were performed.

## **2.9 Cell viability and morphology**

PANC-1, PDX185 and PDX354 cells were seeded and treated as described above for MTT assays. LIVE/DEAD Viability/Cytotoxicity Assay Kit was used according to the manufacturer's instructions. Briefly, cells were incubated with 100  $\mu\text{L}$ /well of a solution containing 1  $\mu\text{M}$  calcein AM and 2  $\mu\text{M}$  EthD-1 in DPBS for 20 minutes in the dark and fluorescence intensity emission was measured at 525 and 645 nm upon excitation at 485 and 525 nm using an Infinite M200 PRO microplate reader. Additionally, images of cultures were taken with an EVOS Digital Colour Fluorescence Microscope. Three independent experiments, each in triplicate, were performed.

## **2.10 Western Blot**

PANC-1, PDX185 and PDX354 cells ( $5 \times 10^5$  cells/well in 6-well plates) were incubated with complete media containing 0.5 mg/mL nanoparticles for 3 or 24 hours. After washing with PBS, cells were lysed with RIPA buffer supplemented with PhosSTOP® phosphatase inhibitor cocktail and COMPLETE® protease inhibitor cocktail, and protein concentration was measured by the Bradford assay. 50  $\mu\text{g}$  of total protein were separated by standard SDS-PAGE and transferred to PVDF membranes. Blocking was performed with 5% BSA in PBS for 1 hour at room temperature. Primary antibodies against total Akt, phosphorylated Akt ( $\rho$ -Akt), phosphorylated c-Jun N-terminal kinase ( $\rho$ -JNK),

nuclear factor kappa-light-chain-enhancer of activated B cells (NF- $\kappa$ B p65), cleaved caspase-3,  $\beta$ -actin and Glyceraldehyde 3-phosphate dehydrogenase (GAPDH) were used according to manufacturer's instructions. Briefly, membranes were incubated with the primary antibody diluted 1:1000 in PBS with 0.5% BSA and 0.1% Tween-20, at 4°C overnight. After extensive washes, secondary antibodies, goat anti-mouse and goat anti-rabbit HRP-linked, were used at 1:10,000 dilution for 1 hour at room temperature. After washing, the specific proteins were detected using an ECL chemiluminescent substrate in a ChemiDoc XRS+ Gel Imaging System (Biorad).

### **2.11 *In vivo* pharmacokinetic analysis**

All animal experiments were conducted in accordance with the institutional guidelines for the care and use of experimental animals of the University of Valladolid (Spain) in accordance with Directive 2010/63/EU (Resolution Number 2010/2/23).

BALB/c mice aged 14-16 weeks (n=5 per group) were injected intravenously with 5 mg/Kg fluorescein-labelled ELR nanoparticles. For the time course analysis, 20  $\mu$ L of blood was collected from the submandibular vein at 1, 2, 3, 4, 5, 6 and 24 hours after injection and immediately diluted into 80  $\mu$ L of heparinised PBS. The blood was centrifuged at 21100 xg for 10 minutes at 4°C and the supernatant was loaded onto a black clear bottom 96-well plate for fluorescence reading using a SpectraMax M5e microplate reader (Molecular Devices) with excitation and emission wavelengths of 494 nm and 518 nm, respectively. Plasma auto fluorescence was determined in negative control (non-injected) mice and subtracted to the samples values. Fluorescence intensity values were converted to concentration by extrapolation from a linear standard curve.

To obtain the pharmacokinetic parameters for the compartmental analysis, the data set of each individual mouse was fit to a one-compartment pharmacokinetic model using SAAM II software (University of Washington, USA).

### **2.12 *In vivo* biodistribution**

BALB/c mice aged 14-16 weeks were injected intravenously via the tail vein with 5 mg/Kg of Cy5-labelled nanoparticles. Fluorescent labelling with Cy5 was used for *in vivo* biodistribution assays to get a better resolution with the IVIS imaging system. After 6 hours, animals were anaesthetised with isoflurane in oxygen (4% for induction and 1.5% for maintenance) and transferred immediately to the IVIS imaging system with continuous anaesthesia during measurement. An untreated mouse was always measured at the same time as a control. Animals were scanned for fluorescence by the IVIS *In Vivo* Imaging System (Perkin Elmer). Excitation and emission wavelengths used were 650 and 670 nm, respectively. Moreover, heart, liver, spleen and kidneys were collected and scanned. Fluorescence of the animals was plotted by subtracting background from an untreated mouse.

### **2.13 Histopathological analysis**

Collected liver, spleen, heart and kidneys from BALB/c mice used for the *in vivo* studies (as described in section 2.13) were processed with an automatic tissue processor (Leica TP1020) and embedded in paraffin blocks. Tissue sections of 4 µm of each organ were stained with haematoxylin and eosin (H&E) following instructions from the manufacturer. Assessment on key parameters of organ microstructure and physiology (liver: steatosis, lobular inflammation, ballooning, fibrosis and portal inflammation; spleen: neutrophils, necrosis and thrombosis; heart: heart myocardial damage; kidneys:

glomerular cellularity, tubular vacuolation, interstitial inflammation, interstitial fibrosis and vessels) were performed at the Royal Free Hospital (London, UK).

#### **2.14 Statistical analysis**

Data are reported as mean  $\pm$  SD (n=3). Statistical analysis were performed by variance analysis in combination with a subsequent analysis using the Bonferroni method. A p-value of less than 0.05 was considered to be statistically significant. \*p < 0.05, \*\*p < 0.01, \*\*\*p < 0.001. Data were handled using the SPSS Statistics software version 20 (IBM).

### **3. Results and discussion:**

#### **ELRs design and physicochemical characterisation**

As previously mentioned, amphiphilic ELRs are able to self-assemble into different structures, depending on their composition, above their transition temperature [53]. In this work, two different polymers were used, both consisting on an amphiphilic backbone formed by a glutamic acid-based hydrophilic block and an isoleucine-containing hydrophobic block (Figure 1). As previously described [49], our therapeutic construct included an Akt-in peptide which inhibits the phosphorylation of the protein kinase Akt at serine 473 [43]. This step is key for Akt cytoplasmic activation and its kinase activity involved in multiple signalling pathways [40]. Moreover, other bioactive sequences were added in order to allow the controlled release of the therapeutic inhibitor in targeted cells. Thus, LAEL sequence was included to facilitate the internalisation of the NP into the cells and to escape from the endosomes/lysosomes, where they accumulate and often drugs get inactivated before they can reach their target [54]. Also, a cathepsin D-sensitive sequence

exclusively recognised by lysosomal proteases [55] and the sequence encoding the H5 peptide [56] were added to allow the escape of the Akt inhibitor from the endo/lysosomes.

The control ELR construct only contained the LAEL sequence and was used to clarify any cytotoxicity resulting from the ELR modules, the internalisation of the NPs and their escape from endo/lysosomes. Both ELR polymers included three lysine residues at the N-terminus, to which different molecules could be linked by covalent binding.



Control: MGKKKPV(LAEL)<sub>3</sub>[(VPGVG)<sub>2</sub>(VPGEG)<sub>10</sub>(VPGVG)<sub>2</sub>] [VGIPG]<sub>60</sub>

Akt-in: MGKKKPV(LAEL)<sub>3</sub>[(VPGVG)<sub>2</sub>(VPGEG)<sub>10</sub>(VPGVG)<sub>2</sub>] [VGIPG]<sub>60</sub>-VQEYVYD-LFHAIAHFHIIHGGWHGLIHGWY- AVTDHPDRLWAWERF

**Figure 1.** Scheme of ELRs composition. The different blocks forming ELR-based polymers are represented in a non-scaled scheme. LAEL sequence facilitates the NP internalisation into the cells. ELR<sub>1</sub> is a hydrophilic block containing isoleucine as guest residue. ELR<sub>2</sub> is a block containing glutamic acid. Cathepsin D-sensitive sequence is recognised by lysosomal proteases and H5 peptide allows the escape of the Akt inhibitor (green block) from the endo/lysosomes at acidic pH. Amino acid sequence of ELR polymers: the colour code identifies the functional peptides of the molecules.

As these two polymers had been previously described [49], physicochemical characterisation was only validated as shown in supplementary Figures S1 and S2. Control and Akt-in polymers showed a similar transition temperature (T<sub>t</sub>) of 15.59°C and 15.23°C, respectively (Figures S1C and S2C), indicating the minor influence of the bioactive sequences, namely LAEL, CatD and H5 in the smart behaviour. DLS results

showed that the control polymer was able to self-assemble into 73 nm-size monodisperse particles, whereas the Akt-in polymer formed carriers of 67 nm of diameter (Figures S3A and S4A). Figures S3B and S4B show the negative surface charge of the nanoparticles (-27 mV) due to the hydrophilic block containing glutamic acid forming the corona. On the other hand, when polymers were fluorescently labelled, neither NP size nor surface charge were altered (Table S2). In conclusion, these results confirmed the physicochemical characterisation previously described [49] and showed that our ELR-based nanoparticles fit all the requirements for its application as drug delivery systems with multiple potential biomedical applications (Table 1).

**Table 1.** Physicochemical characterisation of ELR polymers. Experimental molecular weights were determined by MALDI-TOF/MS. Transition temperatures (Tt) of ELRs dissolved in PBS were measured by DSC. Size (diameter, D<sub>h</sub>) and polydispersity index (PdI) of self-assembled NPs dissolved in PBS were measured by DLS at 37°C. NPs ζ-potential dissolved in ultrapure water type I was measured by DLS at 37°C. Mean ± SD.

	Polymer			Nanoparticle		
	Predicted molecular weight (Da)	Experimental molecular weight (Da)	Tt (°C)	D <sub>h</sub> (nm)	PdI	ζ-potential (mV)
Control	48250	48240	15.59	67.10 ± 2.50	0.093	-27.6 ± 1.3
Akt-in	55330	55390	15.23	73.10 ± 3.20	0.083	-26.7 ± 1.7

### Cellular uptake and localisation of ELR nanoparticles

Once the physicochemical characterisation of ELR-based nanoparticles was completed, the nanoparticle cellular uptake by pancreatic cancer cells was determined by flow cytometry (Figure 2). PANC-1, PDX185 and PDX354 cells were incubated with Cy5-labelled control or Akt-in nanoparticles at 0.5 mg/mL for 3 or 24 hours. Surface charge is one of the most important features of a nanodevice, as this parameter affects the



internalisation rate through the cellular membrane. The cellular membrane possesses negative charge, so neutral and negatively charged nanoparticles are thought to enter into the cells via endocytic pathways [57]. Conversely, cationic carriers tend to cause membrane depolarisation and disruption [58], which leads to a reduction of viability of normal cells. Moreover, cationic NPs are more likely to form aggregates by interacting with proteins present in biological fluids such as blood, increasing their size due to protein corona formation before they reach the target site [59-60]. As described above, both types of NPs (control and Akt-in) showed negative zeta-potential: -27.6 and -26.7 mV, respectively.

Flow cytometry data (Figure 2) showed overlapping histograms for cells treated with Cy5-labelled control and Akt-in NPs. This suggests that the uptake rate for both nanocarriers is similar, as no significant differences between control NPs and NPs carrying the Akt inhibitor were observed. The fluorescence intensity observed in cells treated for 3 hours with NPs was almost identical to 24 hours treatment, indicating that the internalisation of the designed ELR NPs occurred in a short period of time (3 hours) after which a minimal increase in uptake was detected. A similar trend was observed among all cell types analysed (PANC-1, PDX354 and PDX185 cells). Therefore, we can conclude that both control and Akt-in NPs were internalised at a similar rate and the posterior differences detected in cell viability and metabolic activity were only due to the presence of the Akt kinase inhibitor. In Figure 2C-D, cellular uptake of ELR control and Akt-in NPs over time was depicted. Interestingly, a similar amount of ELR nanoparticles was internalised after 3- or 24-hours incubation period. Moreover, PANC-1 cells showed lower internalisation rates than pancreatic cancer patient-derived cells, which could be

explained due to the higher aggressiveness of primary tumour cells compared to established cell lines, displaying an enhanced metabolic activity and internalisation rate.

Once internalisation of the designed ELRs was confirmed, confocal microscopy was carried out to study the subcellular localisation and accumulation of these NPs (Figure 2E-F). As shown in Figure 2E-F, ELR nanoparticles were accumulated inside the cells and their green fluorescence signal co-localised with lysosomes (labelled in red with the lysosomal probe LysoTracker Red). Intracellular lysosomal localisation, in fact, was essential for the accurate action of our nanoconstructs, as the cathepsin D-sensitive sequence included in the ELR needs to be recognised by the lysosomal proteases to facilitate the release of the Akt-in. Moreover, at acidic lysosome pH, the H5 peptide included in the ELRs is designed to trigger the formation of pores in the lysosomal membrane allowing the small Akt inhibitor to be released to the cytoplasm. All of these concatenated steps are key for the effective ELR nanoparticle anti-tumour action. If NPs were not internalised into the lysosomes, the Akt inhibitor would not be released to the cytoplasm and could never reach the target Akt protein. There were no differences in terms of the subcellular localisation of NPs in PANC-1 and PDX cells (data not shown).

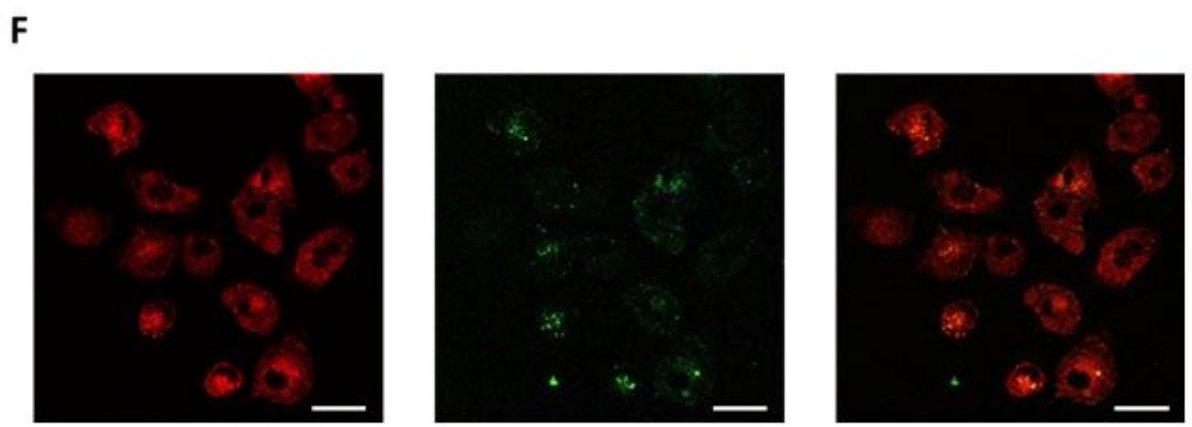
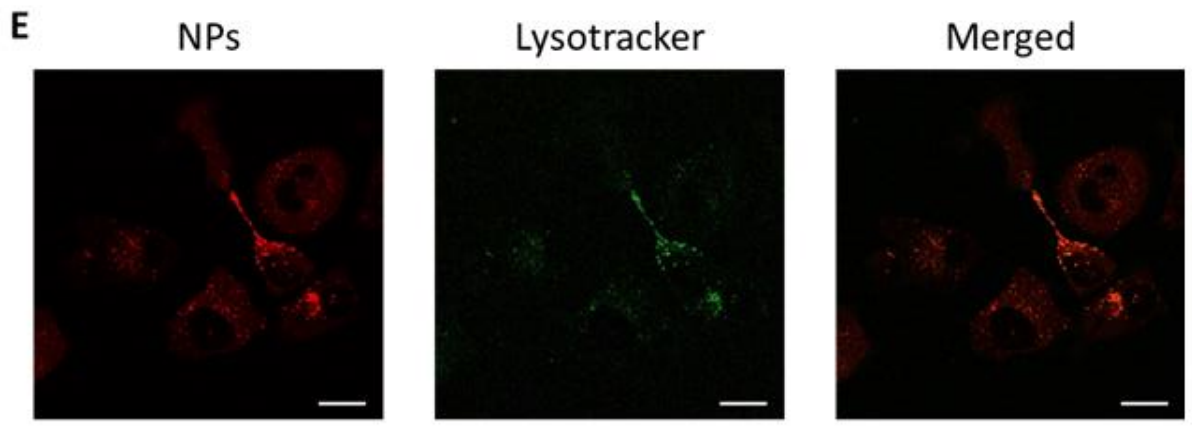
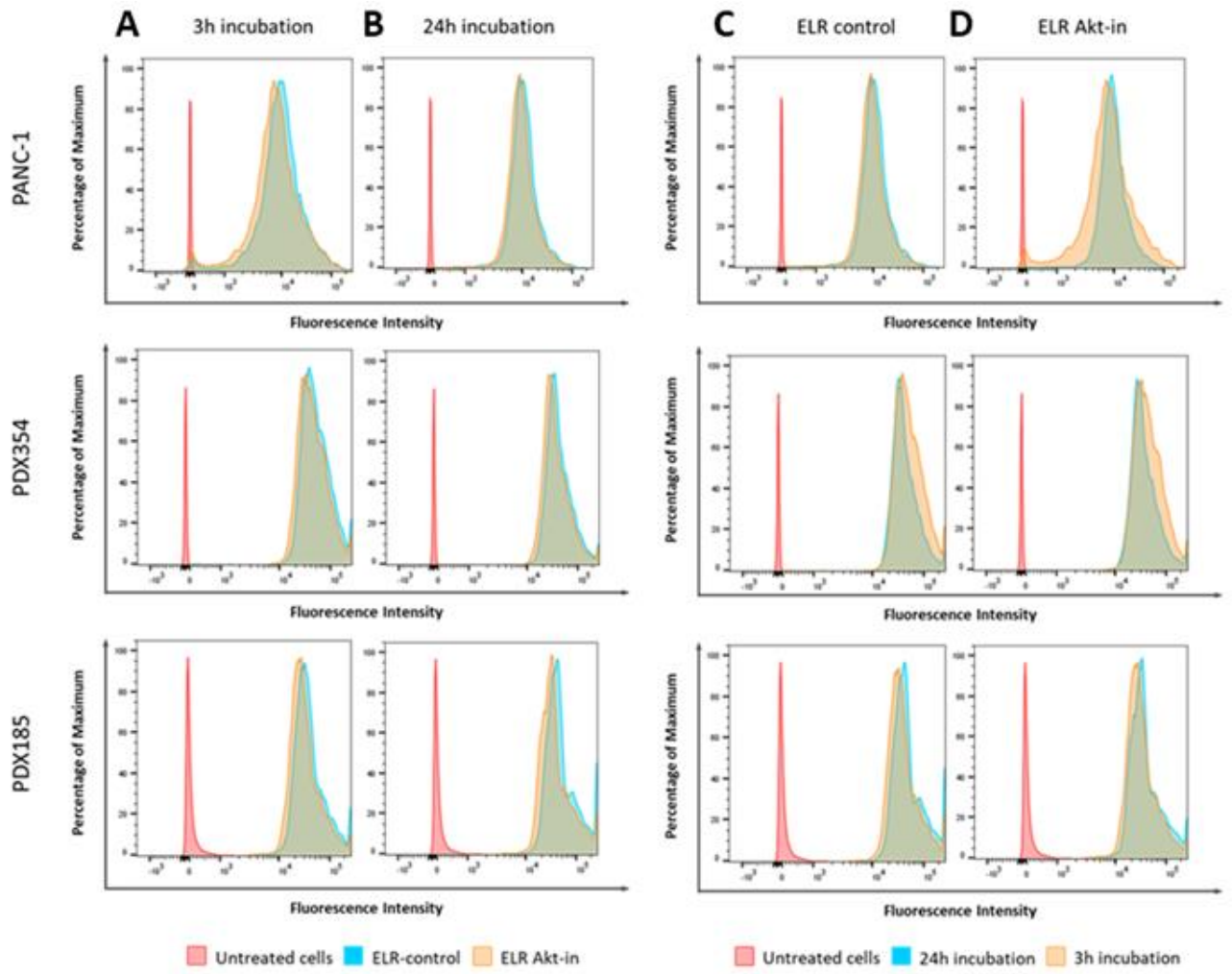


**Figure 2.** Cellular uptake and subcellular localisation of ELR-based nanoparticles in PANC-1 and patient-derived PDX354 and PDX185 cells. A-B: Flow cytometry analysis of cells incubated with control and Akt-in (blue and orange histograms, respectively) Cy5-labelled NPs at 0.5 mg/mL for (A) 3 hours or (B) 24 hours. C-D: Flow cytometry time-course analysis of cells incubated with (C) control or (D) Akt-in Cy5-labelled NPs at 0.5 mg/mL for 3 hours (orange) or 24 hours (blue). Untreated cells are plotted as red histograms. (E-F) Confocal microscopy images of PANC-1 cells containing fluorescein-labelled nanoparticles (green channel) after 3 hours (E) or 24 hours (F). Lysosomes were stained with LysoTracker Red dye (red channel). The overlap of the green and red channels resulted in orange stain. Scale bars: 15  $\mu\text{m}$  (E) and 25  $\mu\text{m}$  (F).

### **Effect of nanoparticles on cellular metabolic activity**

Once the uptake and the localisation of the NPs were determined, their cytotoxic effect was analysed. Previous work from our group demonstrated that control NPs (without the inhibitor) did not affect cell viability and were innocuous for human primary non-cancerous cells, such as fibroblasts, HUVEC endothelial cells and mesenchymal stem cells, whereas an enhanced antitumoural effect was observed on cancerous cell viability [49].

One of the main purposes of drug screening consists of the achievement of predictive models. Although *in vitro* cell culture of established cell lines is a useful tool, the lack of cellular heterogeneity is an important disadvantage. Thus, patient-derived models more accurately mirror the tumour heterogeneity, improving the predictability of therapeutic response to treatment and accelerating the development of novel and more effective therapeutic agents and strategies [61]. Moreover, these models retain most of the morphological and molecular features of the original tumour [62]. For these reasons, we tested our drug delivery systems in pancreatic cancer patient-derived cells.

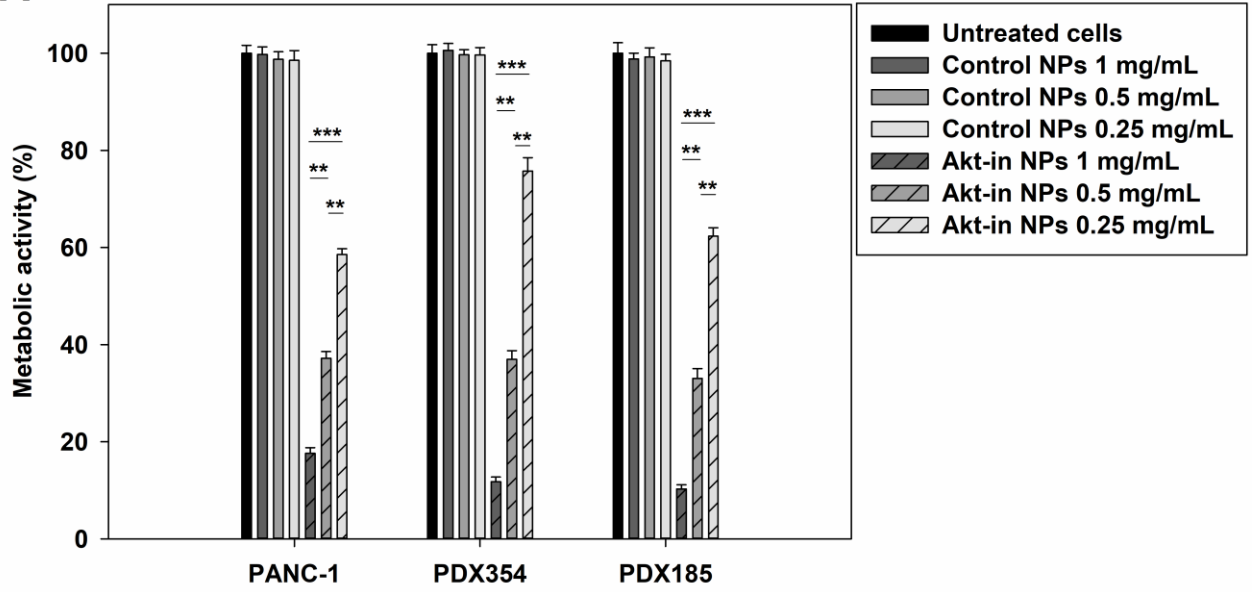
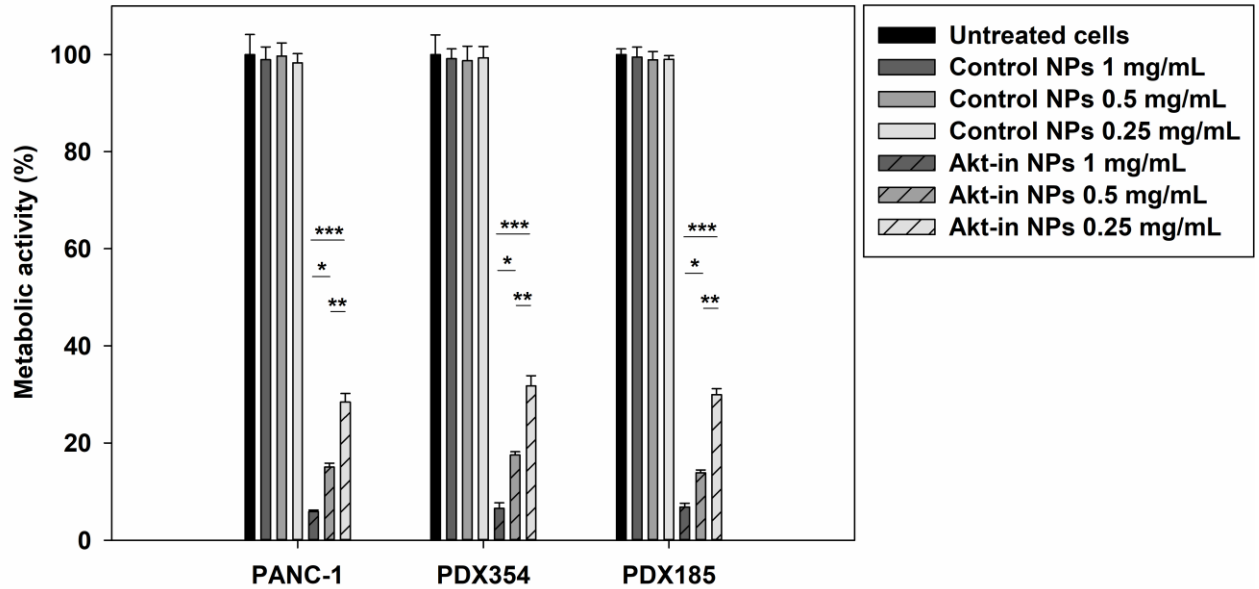
The biological effect of our NPs on the pancreatic cancer cell line PANC-1 and the patient-derived cells PDX185 and PDX354, was determined by evaluating changes in their cellular metabolic activity (Figure 3). Cancer cells were incubated for 3 or 24 hours with three different concentrations of ELR nanoparticles, ranging from the critical micellar concentration (CMC) 0.25 mg/mL to 1 mg/mL. As shown in Figure 3, control NPs did not significantly affect the metabolic activity of any of the cells tested compared to untreated cells. Results showed no difference either between the three different NP concentrations, or between time points. Thus, we can conclude that the basic ELR structure of our nanocarriers did not have any effect on the overall metabolic activity of the pancreatic models used.

Interestingly, when pancreatic cancer cells were incubated with Akt-in ELR nanoparticles for 3 hours, cellular metabolism was affected (see Figure 3A). Metabolic activity was decreased to 58%, 74% and 63% when PANC-1, PDX354 and PDX185, respectively, were incubated with the lowest dose of NPs loaded with the Akt inhibitor (0.25 mg/mL). When the NP concentration was increased to 0.5 mg/mL, the metabolic activity of the 3 cell types dropped to 34-38%. Treatment with the highest NP concentration (1 mg/mL) decreased the metabolic activity to 13-18%. These results not only showed a dose-dependent cytotoxic trend, but also a time-dependent mode of action. It also confirmed that any reduction in metabolic activity observed was due to the presence of the Akt inhibitor and not to the ELR structure.

As expected, when the incubation time with the Akt-in NPs was increased from 3 hours to 24 hours, the cytotoxic effect was enhanced (Figure 3B). Indeed, the highest NP concentration (1 mg/mL) strongly decreased metabolic activity to 4%, 6% and 7% in

PANC-1, PDX354 and PDX185, respectively. Regarding the intermediate NP concentration (0.5 mg/mL), the three cell lines showed only 12-14% of metabolic activity. Lastly, when PANC-1, PDX354 and PDX185 cells were treated with the lowest concentration of Akt-in NPs (0.25 mg/mL), cellular metabolism was decreased to 27%, 31% and 28%, respectively. Thus, results suggest that our NPs improved the cytotoxic effect of the inhibitor on cancer cells in a time- (8 times faster) and dose-dependent manner (5 times lower concentration), compared to the nude inhibitor.

Once the antitumour effect of Akt-in ELR nanoparticles was validated, the percentage of metabolically active cells was measured after allowing cells for any possible recovery for 96 hours after the end of the treatments (Figure 3C-D). As previously observed, control NPs did not affect cellular metabolism, confirming the high biocompatibility of our nanoconstructs. Recovery time slightly decreased the effect of Akt-in NPs on metabolic activity, particularly when using the lowest Akt-in NP concentration and only 3 hours incubation time. When the highest concentration of Akt-in NPs was used (1 mg/mL), cellular metabolism decreased to 22%, 23% and 18% in PANC-1, PDX354 and PDX185, respectively. However, this effect was less significant when cells were incubated for 24 hours with 1 mg/mL Akt-in NPs (cellular metabolism rates of 13-19%), which is in line with our previous results. Interestingly, patient-derived cells showed less metabolic recovery than PANC-1 cells when treated with 1 mg/mL NPs due to the increased NPs internalisation previously observed.

**A****B**

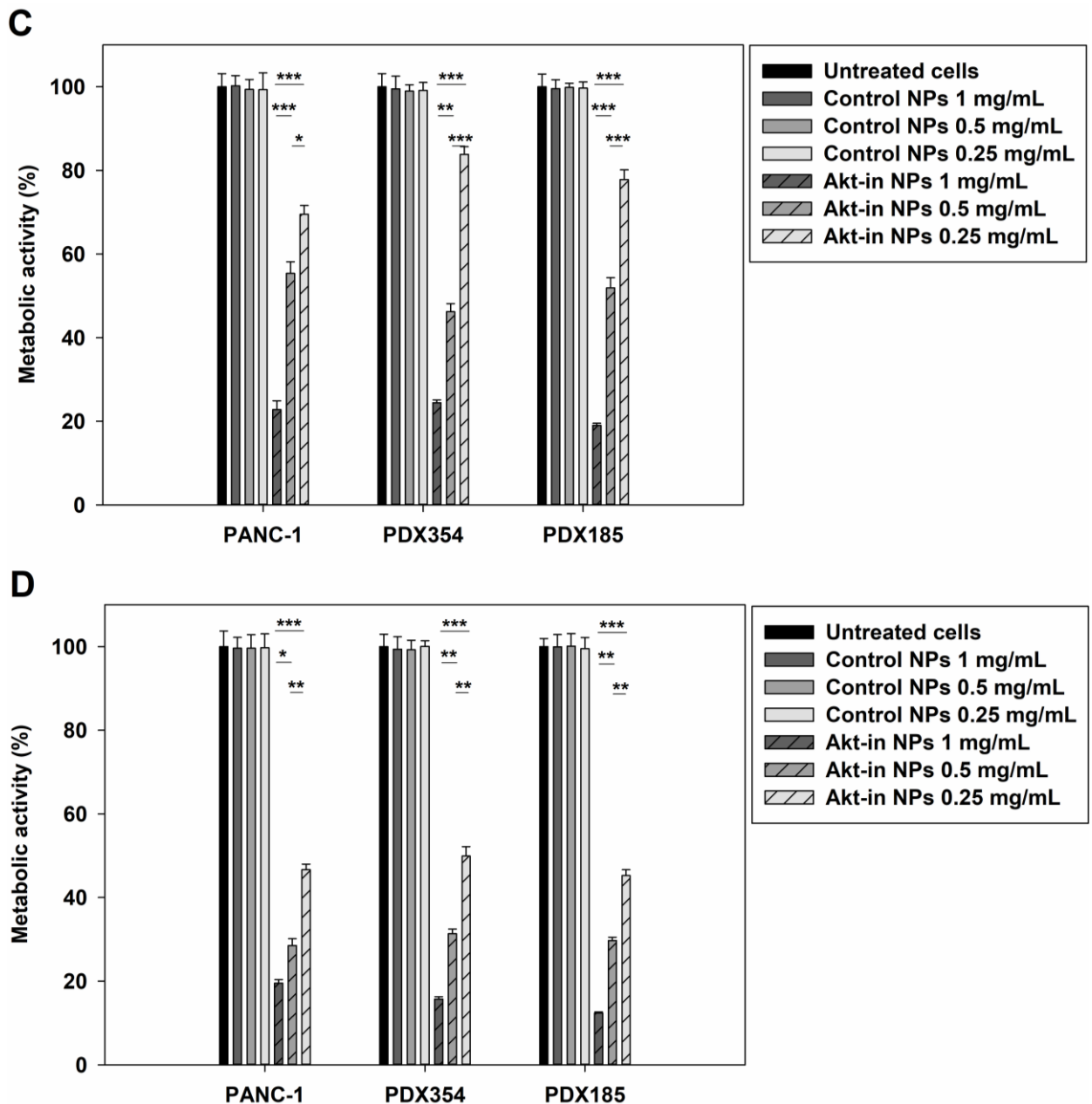


**Figure 3.** Metabolic activity of PANC-1, PDX354 and PDX185 cells after treatment with ELR-based nanoparticles. A-B: Cells were incubated with three concentrations of control and Akt-in nanoparticles for 3 hours (A) or 24 hours (B), and metabolic activity was measured following treatment with NPs using the MTT assay. C-D: Cells were incubated with three concentrations of control and Akt-in nanoparticles for 3 hours (C) or 24 hours (D), media was replaced, and metabolic activity was measured after 96 hours.  $n=3$  independent experiments, mean  $\pm$  SD. \* $p < 0.05$ ; \*\* $p < 0.01$ ; \*\*\* $p < 0.001$ .

### Effect of nanoparticles on cell viability



Once the effect of the different ELR nanoparticles on the metabolic activity of pancreatic cancer cells was determined, cell viability was analysed by the differential staining of live and dead cells with specific fluorescent dyes (Figures 4 and 5). For this purpose, pancreatic cancer cells were incubated under the same treatment conditions of previous experiments. First, the cytotoxic effect of control NPs was determined. Control NPs did not significantly affect the viability of any of the three pancreatic cancer cells lines. Indeed, results showed no difference between the three different concentrations tested at any time point. We can conclude that control NPs were safe and did not induce cell death.

Conversely, when pancreatic cancer cells were incubated with Akt-in NPs, cellular viability was decreased. At a concentration of 0.25 mg/mL, cellular viability was higher than 60% after treating the cells for 3 hours with Akt-in NPs, while when using the intermediate concentration, the three cell lines showed 43-47% viability. When the NP dose was increased to 1 mg/mL, PANC-1 cells and PDX354 showed 25% viability, whereas PDX185 cells were more sensitive and only 17% survived.

Furthermore, we observed that cell viability was dependent on the incubation time with therapeutic ELR nanoparticles. When increasing the incubation time from 3 to 24 hours, results showed that Akt-in NPs were more effective (Figure 4B), matching the MTT data. At lower NP concentrations, PANC-1, PDX354 and PDX185 cells showed 38%, 42% and 34% cell viability, respectively. As expected, cells treated with the intermediate Akt-in NP concentration (0.5 mg/mL) were more affected showing 18%, 26% and 22% cell viability after treatment, for PANC-1, PDX354 and PDX185 cells, respectively. When cells were incubated with the highest concentration of Akt-in NPs (1 mg/mL), the three pancreatic cancer cell lines showed similar values and only 4-7% of cancer cells survived

after treatment. Representative fluorescence microscopy images corroborated the quantitative data obtained.

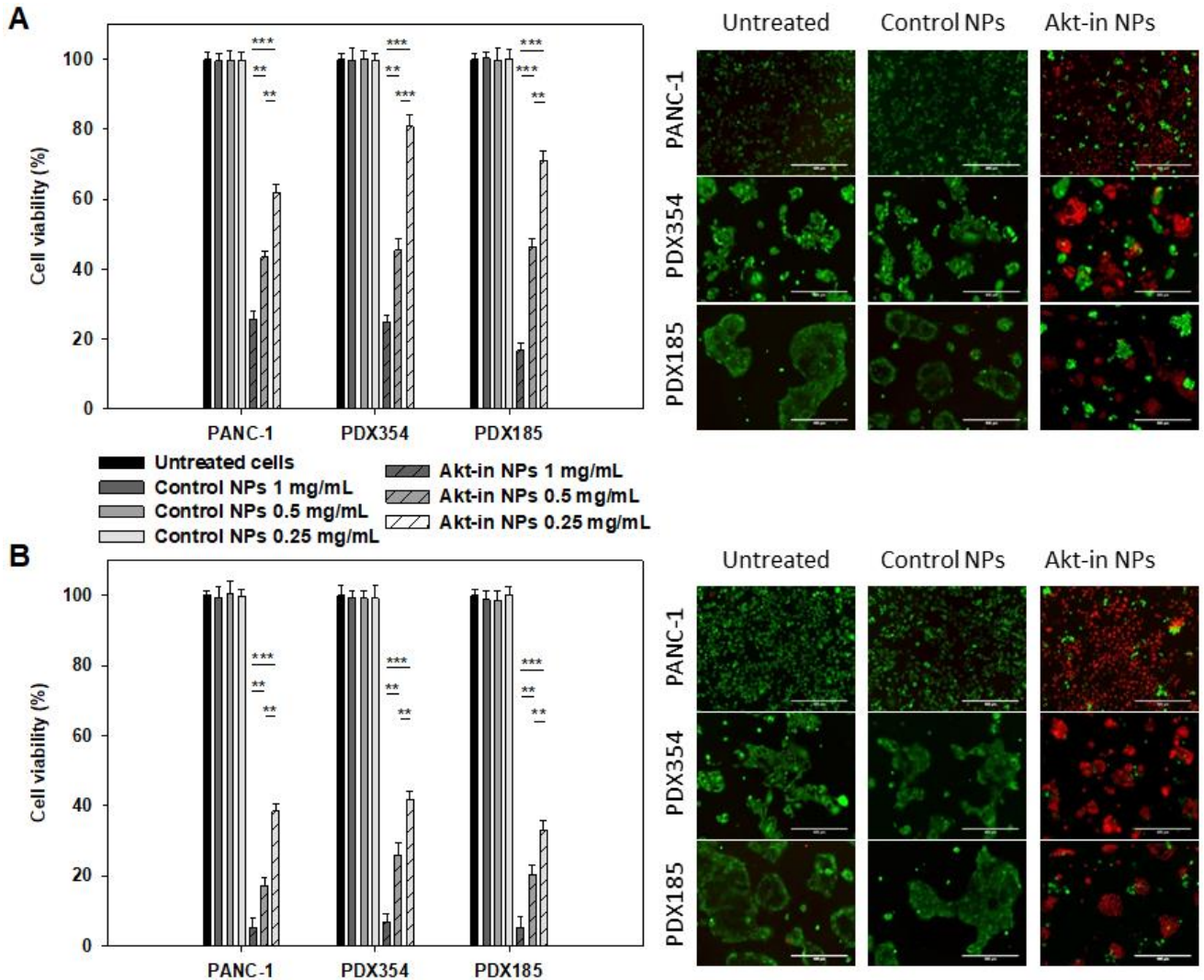


**Figure 4.** Percentage of viability of PANC-1 and patient-derived PDX354 and PDX185 cells compared to untreated cells. Cells were incubated with three concentrations of control and Akt-in nanoparticles for 3 hours (A) or 24 hours (B), and cell viability was measured following treatment with NPs using the LIVE/DEAD assay.  $n=3$  independent experiments, mean  $\pm$  SD. \*\* $p < 0.01$ ; \*\*\* $p < 0.001$ .

The effect of ELR NPs on cell viability was also evaluated 96 hours after treatment for long-term recovery studies (Figure 5). Results confirmed that control NPs were completely innocuous and did not affect cell viability, a key parameter when developing

novel drug delivery systems. When cells were treated with 0.25 mg/mL Akt-in NPs for 3 hours and evaluated 96 hours post-treatment, the three pancreatic cancer cell lines showed viability above 80%. When the intermediate dose was used, the recovery effect was lower, except for PANC-1 cells which showed 67% of cell viability. However, when cancer cells were treated with 1 mg/mL Akt-in NPs, cell recovery was minimal, which corroborated MTT results and validated this concentration as the most effective one.

The percentage of metabolic activity recovery post-treatment was much lower when cells were treated with NPs for 24 hours. Cell viability of PANC-1, PDX354 and PDX185 cells did not reach 60% when treated with the lowest dose of ELR nanoparticles (0.25 mg/mL). When cells were treated with the intermediate concentration, pancreatic cancer cells only recovered 10% proliferation capacity. A significant recovery was not observed when cells were treated with the highest dose, thereby validating the efficacy of our NPs. Hence, these results support that Akt inhibition through our advanced NPs is a promising strategy for the treatment of PDAC and opens the possibility to explore dual or multimodal therapy in combination with chemotherapy to advance clinical translation.

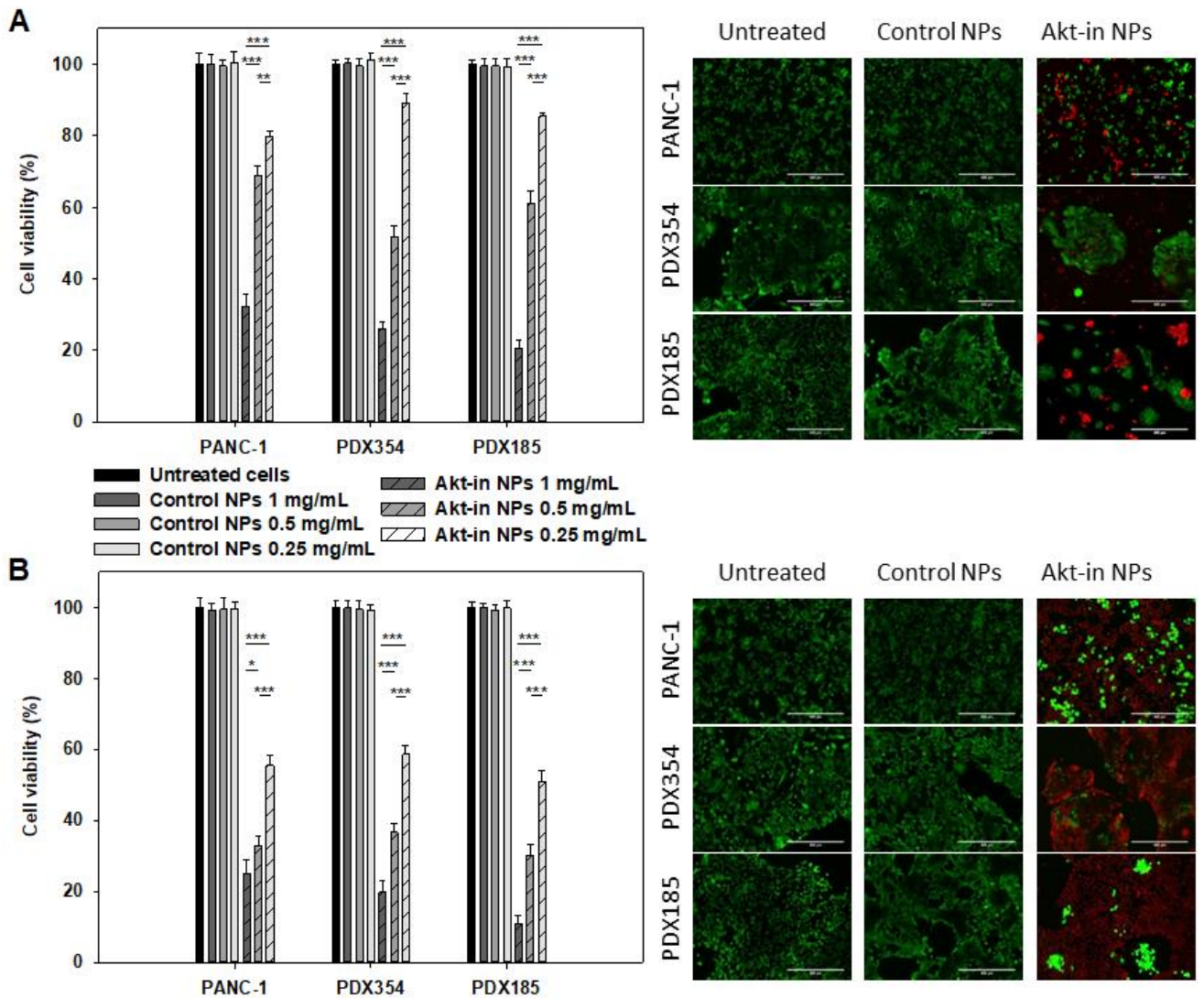


**Figure 5.** Percentage of viability of PANC-1 and patient-derived PDX354 and PDX185 cells compared to untreated cells. Cells were incubated with three concentrations of control and Akt-in nanoparticles for 3 hours (A) or 24 hours (B). Media was refreshed and cell viability 96 hours after treatment was measured using the LIVE/DEAD assay kit. Representative fluorescence microscopy images. Scale bars: 100  $\mu$ m. n=3 independent experiments, mean  $\pm$  SD. \*\*p < 0.01; \*\*\*p < 0.001.

Based on our previous results, the intermediate concentration of ELR-based NPs was selected for further experiments, as this dose affected metabolic activity and cell viability in primary pancreatic cancer cells. Moreover, previous work determined that a dose of 0.5 mg/mL markedly affected breast and colorectal cancer cells viability without

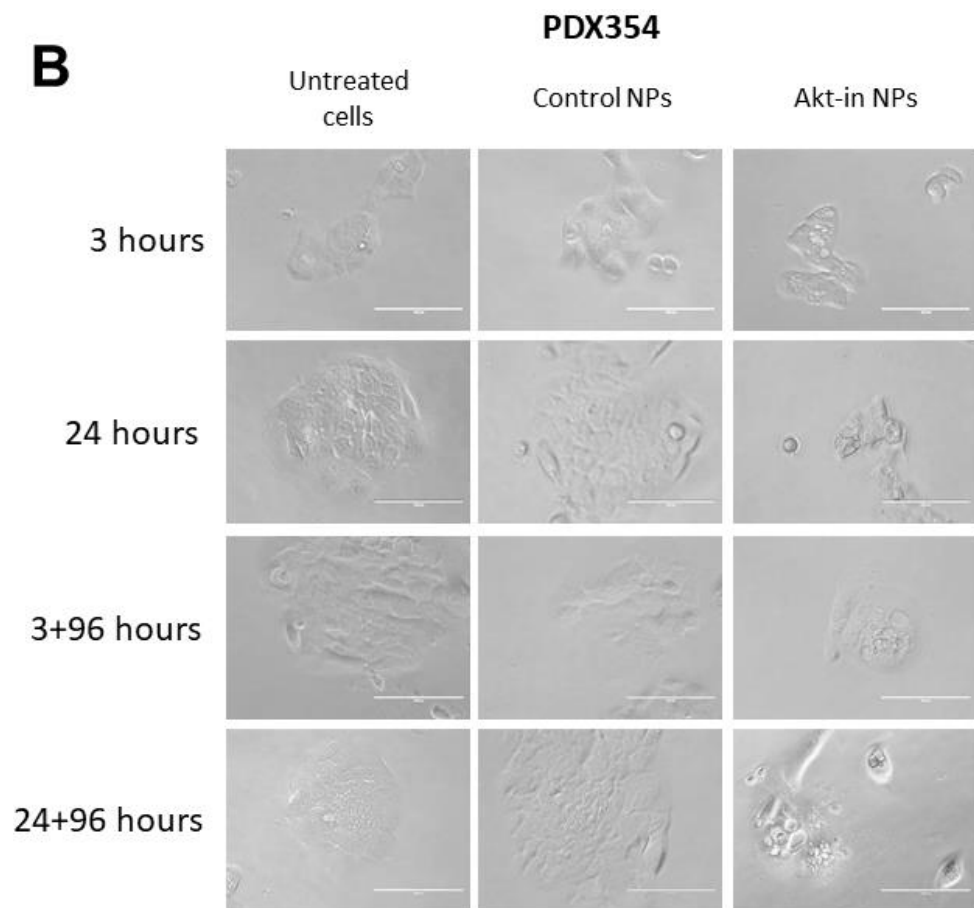
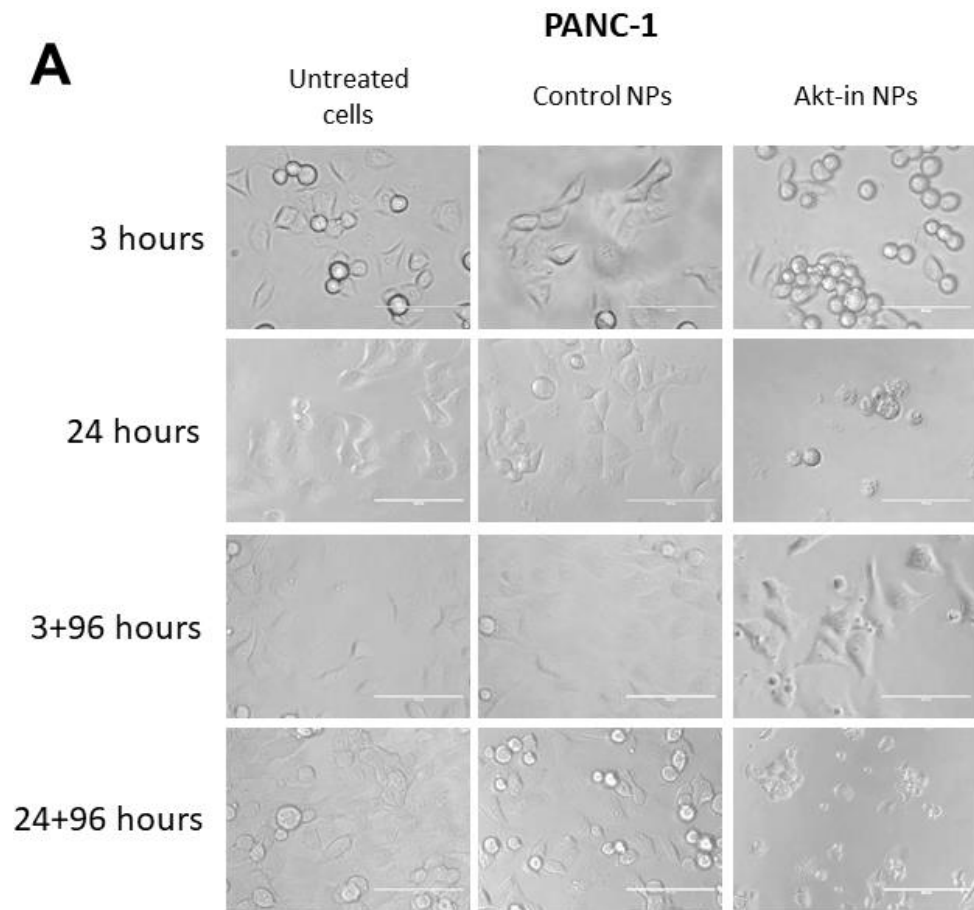
significant effects in primary non-cancerous cells, such as fibroblasts, endothelial and mesenchymal stem cells [49].

### **Effect of nanoparticles on cellular morphology**

After determining the effect of ELRs nanoparticles on cell viability, proliferation and metabolic activity, cellular morphology was also studied to corroborate how pancreatic cancer cells were affected by the treatment with our smart nanocarriers (Figure 6). PANC-1, PDX185 and PDX354 cells were incubated with 0.5 mg/mL ELR nanoparticles for 3 and 24 hours and cell morphology was evaluated.

No major differences in cellular morphology and cell density were observed in any of the three lines incubated with control NPs compared to untreated controls, at any of the selected incubation times. PANC-1 cells (Figure 6A) showed a higher sensitivity to the 3 hours treatment with NPs containing the inhibitor than PDXs, corroborating the data obtained by MTT and LIVE/DEAD assays. Treatments for 24 hours with Akt-in NPs showed a complete disruption of the normal pattern of growth and colony formation capacity of the three cell types. The few surviving cells after 24 hours of treatment displayed a round morphology typical of cells undergoing cell death, which strongly supports the higher effect in cell viability previously observed.

In experimental conditions where cells were treated for 3 or 24 hours and then media was refreshed to allow for any possible recovery during the next 96 hours, pancreatic cancer cells, namely PANC-1, PDX354 and PDX185, showed a strong decrease in cell density suggesting that no major cell recovery happened after treatment.



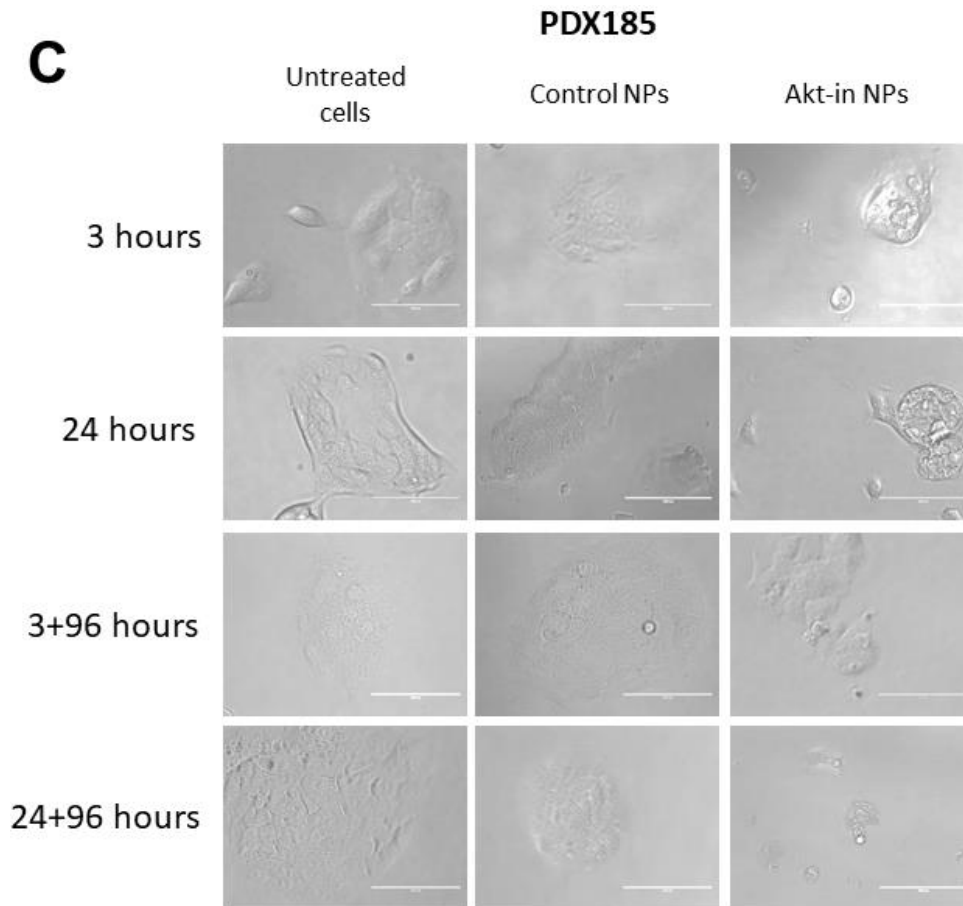


**Figure 6.** Cell morphology of PANC-1 (A), PDX354 (B) and PDX185 (C) cells treated with ELR-based nanoparticles. Cells were incubated with control and Akt-in nanoparticles at 0.5 mg/mL in culture media for indicated times; from top to bottom: 3 and 24 hours incubation with nanoparticles, 3 and 24 hours incubation with nanoparticles + 96 hours in culture medium without nanoparticles. Pictures were taken by optical phase contrast microscopy. Representative images. Scale bars: 100  $\mu$ m.

#### **Action of Akt inhibition on cell signalling pathways**

As described above, the primary aim of this work was to achieve a controlled delivery of the small peptide inhibitor of the phosphorylation of Akt to the cellular cytoplasm. In this regard, the expression of certain proteins involved in cell signalling pathways controlled by Akt was studied to confirm the NPs mechanism of action and their accurate effect in Akt phosphorylation.

Akt protein, once phosphorylated at the threonine and serine residues, becomes active and plays a key role in multiple cell signalling pathways summarised in Figure 7. Thus, Akt kinase controls cell growth, proliferation and survival [36-37] and its higher expression correlates with poor prognosis and lower survival rates in pancreatic cancer patients (Figure 7) [63], thereby making Akt a promising target for cancer therapy.

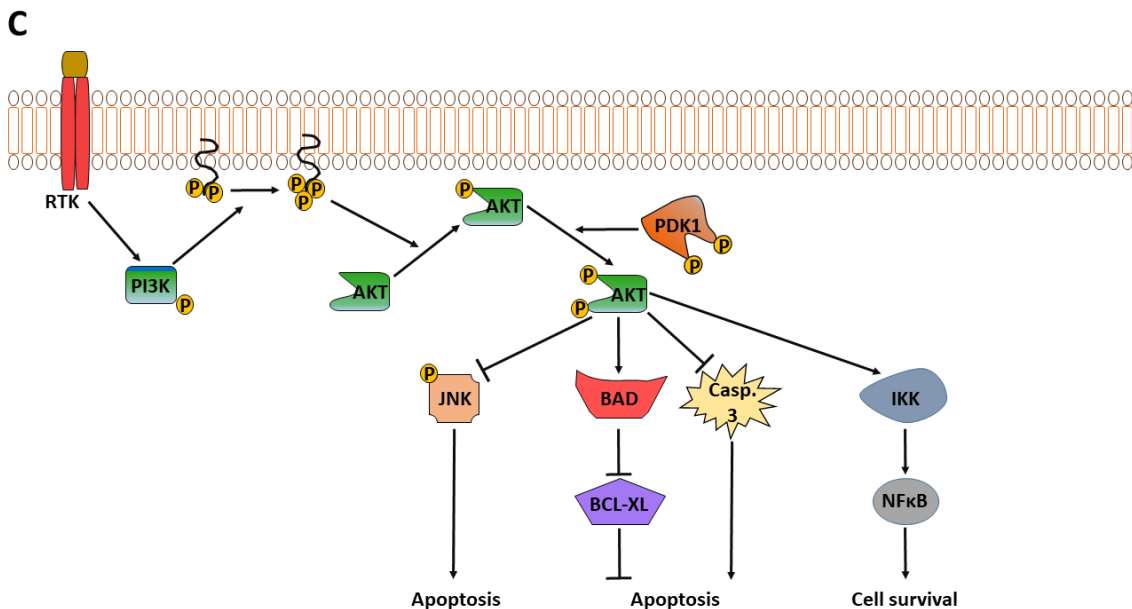
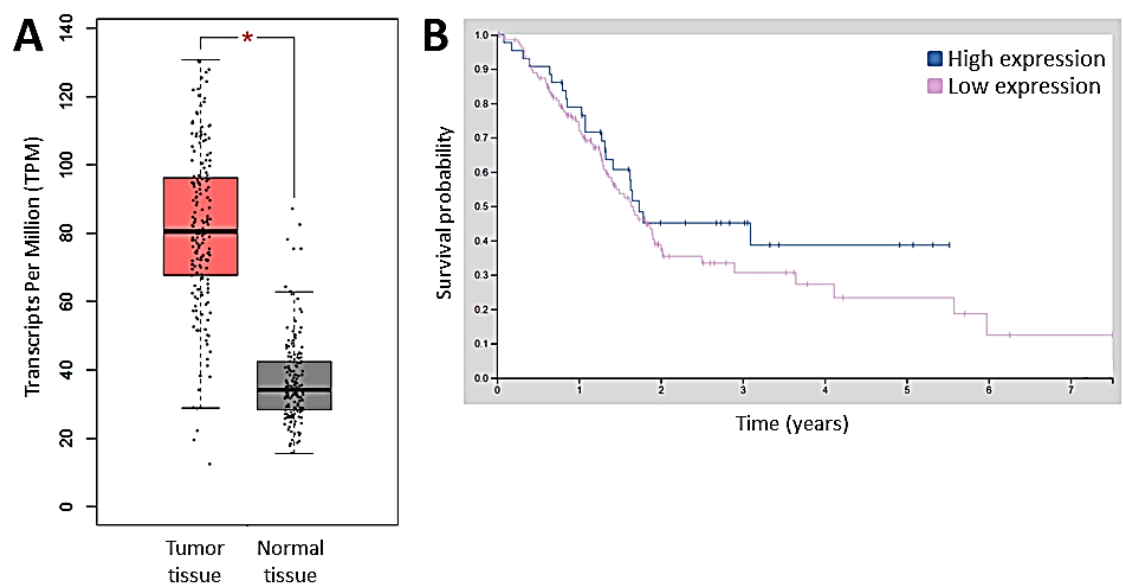


**Figure 7.** A: Differential expression of Akt in pancreatic tumour and normal tissues. Adapted from [63]. B: Kaplan-Meier survival plot for pancreatic cancer where high expression of Akt has significant ( $p < 0.001$ ) association with patient survival. Adapted



from [63]. C: Cell signalling pathways involving Akt kinase. Akt is phosphorylated by PI3K and PDK1. Active Akt kinase plays important roles in multiple signalling pathways regulating apoptosis or cell survival.

As our advanced drug delivery system carried a small inhibitor of Akt phosphorylation and consequent activation, immunoblots were performed to check the mechanism of action of the inhibitor released from the NPs. Expression levels of several proteins involved in cell signalling pathways regulated by Akt were also evaluated (Figure 8). Pancreatic tumour cells showed serine 473 phosphorylated Akt kinase, which corroborated the fact that cancerous cells have this signalling pathway constitutively activated. As expected, when cancerous cells were treated with control nanoparticles, the phosphorylation of Akt protein was not altered after 3 (Figure 8A) or 24 hours (Figure 8B). However, Akt phosphorylation was markedly inhibited when cells were incubated with Akt-in NPs after both incubation times. Furthermore, expression levels of total Akt protein did not change after treatment with control nanoparticles or with Akt-in NPs in PANC-1, PDX354 and PDX185 cells.

Even though the blockade of Akt phosphorylation and activation was demonstrated, we also measured the downstream effect of inhibiting Akt in pancreatic cancer cells, to corroborate the action of Akt-in NPs over cell signalling. Nuclear factor kappa-B, NF $\kappa$ B transcription factor, is located downstream in the Akt signalling pathway and is activated by phosphorylated Akt kinase (Figure 7) [64]. Since NF- $\kappa$ B protein regulates cell survival, which is a key hallmark of cancer cells, NF- $\kappa$ B expression levels were measured [65]. Figure 8 shows untreated pancreatic cancer cells displaying a high expression of NF- $\kappa$ B. These expression levels were not altered when PANC-1 and patient-derived pancreatic cancer cells were treated with control NPs. On the contrary, when pancreatic

cancer cells were incubated with ELRs nanoparticles carrying the Akt inhibitor, expression levels of NF- $\kappa$ B decreased. The effect of Akt-in NPs on decreasing NF- $\kappa$ B expression was validated after treating pancreatic cancer cells for 3 (Figure 8A) or 24 hours (Figure 8B). This result corroborated the fact that Akt phosphorylation, and consequent activation and signalling, was properly inhibited and cell survival controlled by NF- $\kappa$ B was also blocked by treating the cells with our Akt-in loaded NPs.

In a previous work, we demonstrated that breast and colorectal cancer cells underwent apoptosis after treatment with Akt-in NPs [49]. We hypothesised that when NPs were able to inhibit the anti-apoptotic effect of Akt activation, cancerous cells would undergo apoptosis-mediated death. For this reason, cleaved caspase 3 expression levels were evaluated in our pancreatic models as this protein plays a key role in apoptotic cell death [66-67]. Cleaved caspase 3 was not detected 3 hours after treatment (data not shown), however, it was detected 24 hours after treatment (Figure 8B). Results proved that untreated cells, which possessed aberrant growth, showed no cleaved caspase 3 expression. When pancreatic cancer cells were incubated with control NPs, active caspase 3 expression was not increased. These results suggest that control NPs were completely innocuous for cell viability. As it can be seen in Figure 8B, caspase 3 was only cleaved when pancreatic cancer cells were incubated with NPs carrying the Akt inhibitor. Thus, we could conclude that effective inhibition of Akt phosphorylation and activation allowed pancreatic cancer cells to undergo apoptosis-mediated death.

Moreover, phosphorylation levels of the JNK protein were determined after 24 hours of incubation with ELR-based nanoparticles (Figure 8B), as this pro-apoptotic protein is inhibited by phosphorylated Akt kinase in cancer cells (Figure 7) [68-69]. Western Blot

results showed that phosphorylation and consequent activation of JNK protein was not altered by the incubation with control NPs. However, enhanced phosphorylation levels of JNK protein were detected when the activation of Akt kinase was inhibited by ELRs nanoparticles carrying the small inhibitor. These results demonstrated that the accurate mode of action of NPs over Akt protein was not only due to the inhibition of its phosphorylation, but also due to the blockade of cell survival signalling controlled by the NF- $\kappa$ B pathway, and the subsequent activation of the p-JNK pathway leading to caspase 3-mediated cell apoptosis. Moreover, apoptotic death of pancreatic cancer cells treated with Akt-in NPs was corroborated by measuring cleaved caspase-3 expression.

Treatment	PANC-1			PDX354			PDX185		
Control NPs	-	+	-	-	+	-	-	+	-
Akt-in NPs	-	-	+	-	-	+	-	-	+

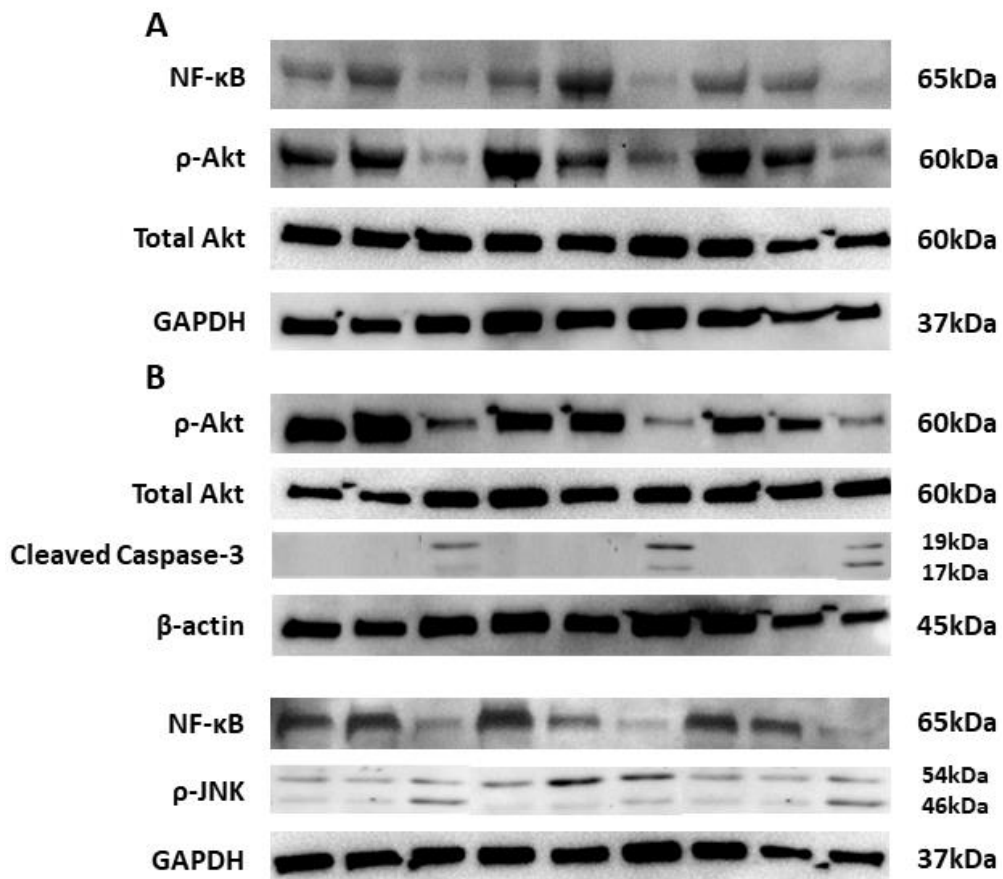


**Figure 8.** Effect of ELR nanoparticles on cell signalling pathways involving Akt kinase. PANC-1, PDX354 and PDX185 cells were incubated with 0.5 mg/mL control or Akt-in nanoparticles for 3 (A) or 24 hours (B). Immunoblots were performed to measure expression levels of NF- $\kappa$ B, Akt phosphorylation at Ser473, total Akt, cleaved caspase-3 and  $\rho$ -JNK. Glyceraldehyde 3-phosphate dehydrogenase (GAPDH) and  $\beta$ -actin were used as loading controls.

### ***In vivo* pharmacokinetic profile of ELR-based nanoparticles**

Short circulating half-life is the main disadvantage of therapeutic agents, such as chemotherapeutic drugs or peptides. This requires repeated administration of high concentrations to obtain therapeutically effective levels which usually result in high toxicity and off-target effects in healthy tissues [70-71]. Therapeutic molecules need to overcome several biological barriers to reach the target tissue and ensure an effective dose. ELR-based carriers play an interesting role overcoming all these limitations as they are able to extend the circulating half-life of therapeutic peptides or drugs and also improve their specific accumulation and pharmacokinetics [14].

The pharmacokinetic profiles of control and Akt-in NPs was compared after intravenous administration of fluorescein-labelled ELRs in BALB/c mice and collection of blood samples at various time points. Figure S5 shows the plasma concentration versus time curve for both ELR polymers and one-phase decay behaviour was observed. Therefore, the one-compartmental model was used to fit the plasma concentration-time curve by SAAM II software. This model assumes that the whole body acts like a single uniform compartment, the drug is distributed instantaneously throughout the entire body and drug elimination occurs immediately after the intravenous bolus injection [17, 72].

Pharmacokinetic parameters were determined and are shown in Table 2. The distribution volume of control and Akt-in NPs was almost the same than blood volume of a mouse. These values indicate that ELR nanoparticles were not rapidly accumulated in organs and tissues after administration. As presented in Table 2, ELR-based nanoparticles showed long half-life (5.8 and 5.3 hours for control and Akt-in NPs, respectively), similar to previous ELRs developed for drug delivery purposes [73-75]. Moreover, no statistical difference was observed in any parameter when comparing control and Akt-in NPs, which indicates that both nanoparticles have similar *in vivo* distribution and elimination profiles. These pharmacokinetic parameters are considered suitable features in terms of delivery of therapeutic agents and drugs [17, 73]. These results indicate that our novel advanced NPs are suitable biomaterials for drug delivery purposes and future drug response studies.

**Table 2.** Pharmacokinetic parameters of intravenously administered control and Akt-in nanoparticles. One compartment analysis. Mean  $\pm$  SD. Abbreviations: AUC: Area under the curve, F: Bioavailability, CL: Clearance, Vd: Volume of distribution,  $T_{1/2}$  elimination: Terminal half-life,  $K_{\text{elimination}}$ : elimination rate constant.

	<b>Control NPs</b>	<b>Akt-in NPs</b>
AUC ( $\mu\text{m}\cdot\text{h}$ )	148 $\pm$ 8	129 $\pm$ 12
F (%)	100	100
CL (mL·h)	0.22 $\pm$ 0.08	0.25 $\pm$ 0.04
Vd (mL)	1.8 $\pm$ 0.3	1.9 $\pm$ 0.5
$T_{1/2}$ elimination (h)	5.8 $\pm$ 0.4	5.3 $\pm$ 0.6
$K_{\text{elimination}}$ ( $\text{h}^{-1}$ )	0.12 $\pm$ 0.02	0.13 $\pm$ 0.02

### ***In vivo* biodistribution**

*In vivo* biodistribution of our NPs was also evaluated in mice (Figure 9). The pharmacokinetic profile of ELR-based nanoparticles showed that our nanocarriers could be a suitable device for drug delivery purposes presenting appropriate distribution volume (Vd) and half-life. For this reason, the biodistribution of the carriers was studied in order to determine whether the NPs get preferentially accumulated in any specific organ upon intravenous administration. Briefly, ELR-based polymers were labelled with Cy5 as described above. Cy5-labelled nanoparticles were injected intravenously into BALB/c mice and the biodistribution was monitored using the IVIS *In Vivo* Imaging System after subtracting background from an untreated mouse. Moreover, heart, spleen, liver and kidneys were collected and scanned.

Figure 9A shows an increased accumulation of NPs in the gastrointestinal tract (GIT) 6 hours post injection. GIT has been proposed as one of the major organs for nanomaterials interaction and uptake [76-79]. Thus, several GIT features play a role in this, such as the presence of enterocytes or the mucus layer [80-82]. Moreover, intestinal mucus secretion enhances nanomedicine transportation and uptake by endocytosis-mediated pathways [83]. One of the main problems of NPs for drug delivery purposes is their accumulation in critical organs such as heart, liver or kidneys. NPs bigger than 100 nm are able to escape from liver capture [84]. Also, particles smaller than 10 nm suffer from renal clearance [24]. Therefore, nanoparticles with sizes ranging from 10 to 100 nm are preferred [85-86]. In this work, our ELR-based NPs showed sizes of 67 and 73 nm for control and Akt-in nanodevices, respectively. Remarkably, there was no signal detected in liver or kidneys (Figure 9B). Furthermore, there was no heart accumulation (Figure 9B). This is important, as some of the side effects of current chemotherapeutic drugs are due to cardiac toxicity [7]. In this context, and taking into account our results, we could

conclude that the developed ELR-based nanoparticles are suitable drug delivery nanosystems because no accumulation was appreciated in critical organs.

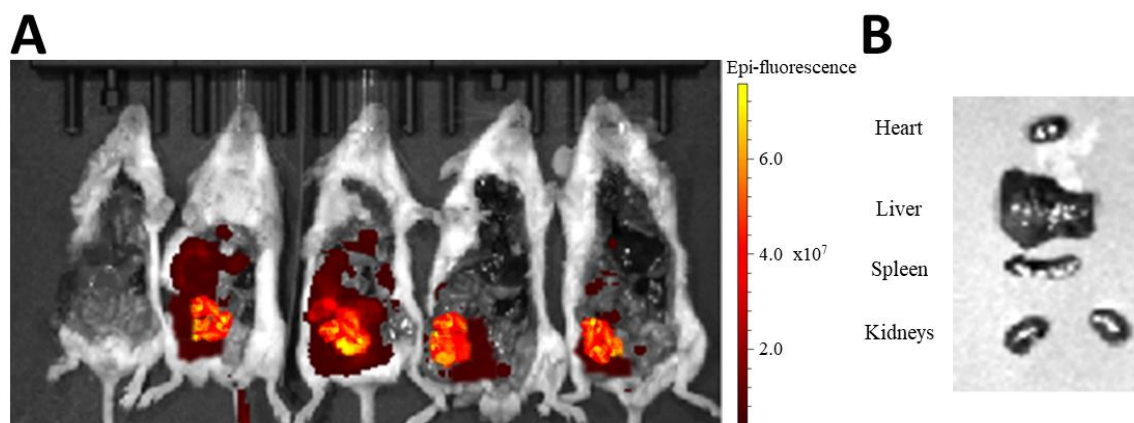


**Figure 9.** *In vivo* imaging of the biodistribution of Cy5-labelled NPs into BALB/c mice. Cy-5 labelled ELR nanoparticles were systemically injected via tail vein. After 6 hours, animals were sacrificed and transferred immediately to the IVIS imaging system. A: Untreated animal (first from left) was measured as control. The other four animals were injected intravenously with 5 mg/Kg Cy5-labelled NPs via tail vein. B: Heart, liver, spleen and kidneys from treated animals were collected and their fluorescence was scanned in order to determine the nanoparticle accumulation within the different organs.

### **Histopathology examination of liver, kidney, heart and spleen**

The pharmacokinetic profile and organ biodistribution of our ELR-based nanocarriers confirmed their potential safety as no critical accumulation was observed in key organs. An analysis of the organ microstructure was also performed to check for any internal damage that may have arisen upon injection of control and Akt-in containing NPs into the mice. In this regard, sections from key organs including liver, kidney, spleen and heart were stained with H&E (Figure 10) and assessed on key parameters of organ microstructure and physiology, such as i) liver: steatosis, lobular inflammation, ballooning, fibrosis and portal inflammation; ii) spleen: neutrophils, necrosis and thrombosis; iii) heart: heart myocardial damage; and iv) kidneys: glomerular cellularity,

tubular vacuolation, interstitial inflammation, interstitial fibrosis and vessels. Liver assessment was based on non-alcoholic fatty liver disease (NAFLD) activity score (NAS) type scoring [87]. Spleen assessment was based on methodology described by Gibson-Corley *et al.* [88] and heart score was based on a system developed by Sachdeva *et al.* [89]. The results obtained from the examination did not show significant differences and only minor abnormalities were observed in organs of mice treated with control or Akt-in NPs, thereby highlighting the safety and tolerability of our nanocarriers as drug delivery systems (Figure 10).

These results corroborate previous findings on the safety of the nanocarriers which did not generate major deterioration on organs typically affected by free or encapsulated drugs. In addition, it was confirmed that the incorporation of the Akt inhibitor to the nanoconstructs did not change the mode of action of the nanomedicine compared to its analogous control nanoparticles.



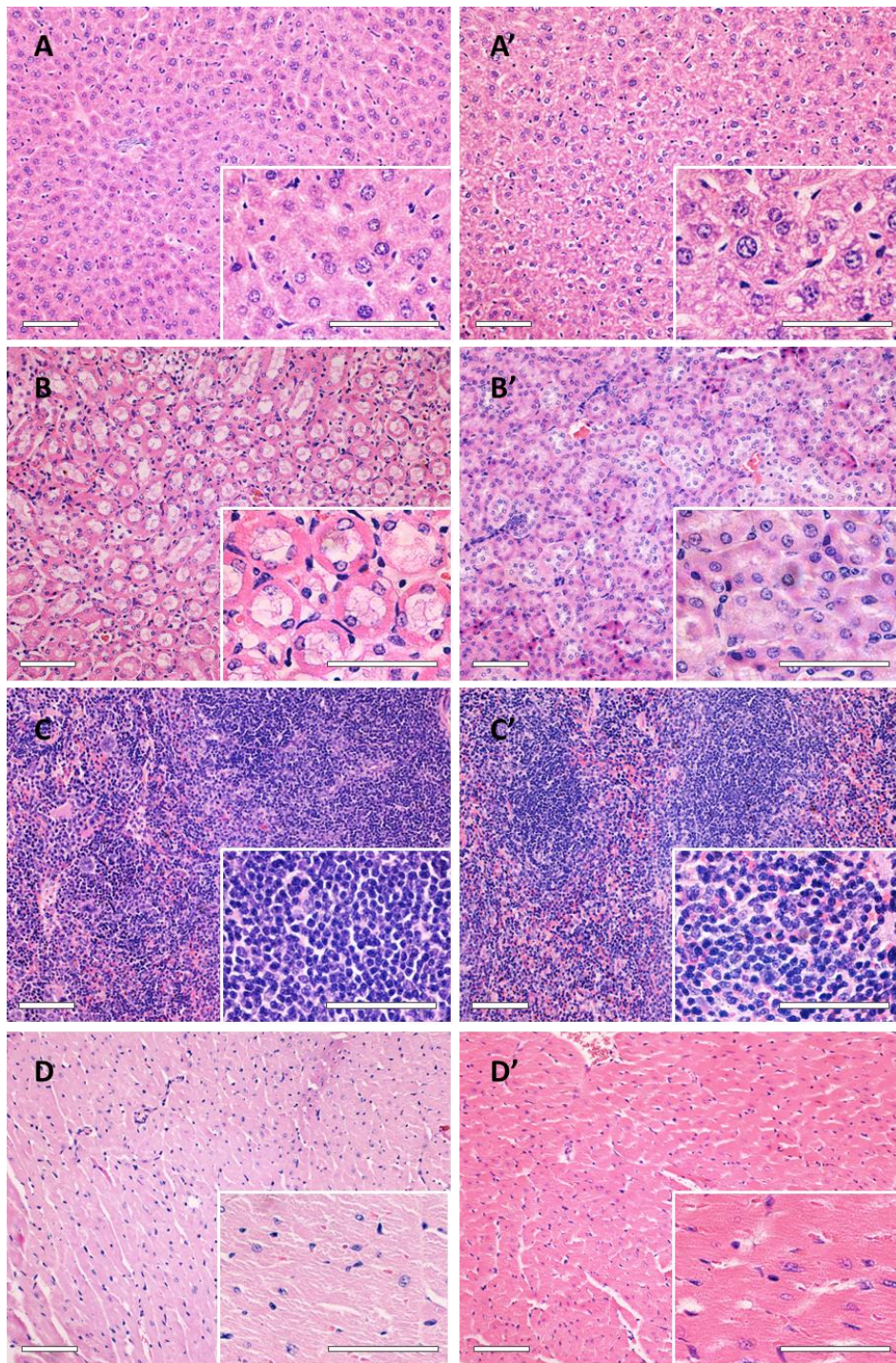


**Figure 10.** Effect of the nanoparticles injection on organ histology. Selected organs from BALB/c mice treated with control (A-D) or Akt-in NPs (A'-D'). A: Liver; B: Kidney; C: Spleen and D: Heart. Scale bars: 50  $\mu$ m.

#### **4. Conclusions:**

Low specificity, off-target side effects and poor drug accumulation in the target site due to the difficult access to the tumour, particularly in desmoplastic lesions such as pancreatic cancer, are major hurdles in cancer therapy leading to limited success of current drugs. Nanotechnology appears as a promising approach for controlled drug delivery and optimal-dose reduction of therapeutic drugs.

In this work, we took advantage of ELR polymers to create advanced NPs with high conformational complexity for controlled drug delivery. The 73 nm NPs carried a small fifteen amino acid peptide which bound to the cytoplasmic Akt protein inhibiting its activation, as well as different bioactive sequences to facilitate their internalisation, the enzymatic release of the inhibitor and the escape from the endo/lysosomes to the cellular cytoplasm to reach its target.

The NPs anti-tumour activity was evaluated in pancreatic cancer patient-derived models and our results showed that both control and Akt-in NPs, were internalised and accumulated within the lysosomes, where the escape sequences were designed to act in order to release the inhibitor to the cytoplasm. Results also demonstrated that Akt-in NPs not only reduced cellular metabolic activity but also pancreatic cancer cell viability. In fact, cancer cells underwent apoptosis. Contrarily, control NPs did not impact cell metabolism nor viability. Based on our results, we can conclude that our NPs inhibited the Akt signalling pathway and consequently, blocked cell survival controlled by the NF- $\kappa$ B pathway. Thus, these smart NPs were shown to be an accurate and promising drug delivery system for controlled release in pancreatic cancer cells.

*In vivo* pharmacokinetic profiling showed that both control and Akt-in NPs have long half-life and proper distribution volume, which suggested that they are suitable drug delivery devices for systemic administration. Furthermore, *in vivo* assays showed that the NPs did not accumulate in critical organs, damage their microstructure or alter their normal physiology, some of the most common disadvantages leading to low accuracy and undesired side effects.

To the best of our knowledge, this is the first time that NPs carrying an Akt inhibitor are evaluated for therapeutic purposes in pancreatic cancer patient-derived models. As Akt protein is not only overexpressed in pancreatic, but also in other multiple types of cancer, different studies could be potentially accomplished to test the efficacy of this nanodevice in other cancer models. Even though we studied the accuracy of these NPs in clinically relevant patient-derived models, further studies are needed to determine the effectiveness of these NPs *in vivo*, before moving into clinical trials. Thus, a dual combination approach could be explored involving both, self-assembling NPs encapsulating our Akt inhibitor and chemotherapy. In the future, cancer patients overexpressing the Akt protein may be good candidates for clinical studies with NPs carrying an Akt inhibitor, which could improve the problems caused by current unspecific chemotherapeutic drugs.

### **Supporting Information**

Physicochemical characterisation, including HPLC, MALDI-TOF, DSC, <sup>1</sup>H-NMR and DLS spectra for all compounds. Pharmacokinetic profiles after systemic administration of nanomaterials in BALB/c mice.

### **Conflict of interest**

The authors declare no competing financial interest.

## **Funding**

This work was supported by funds from Pancreatic Cancer UK (PCUK), the European Social Fund (ESF), the European Regional Development Fund (ERDF) and the MICIUN (grant numbers MAT2016-79435-R, DTS19/00162 and PID2019-106386RB-I00). J. G.-V. was supported by the University of Valladolid as well as the Erasmus+ programme of the European Union through a travel fellowship for PhD students. P. A. was supported by a Postdoctoral Fellowship from the Ramón Areces Foundation.

## **Acknowledgments**

The authors would like to thank R. Garcia for her technical assistance with polymers bioproduction and R. Alvarez-Delgado for her assistance with animal procedures.

## **5. References**

1. Vincent, A.; Herman, J.; Schulick, R.; Hruban, R. H.; Goggins, M. Pancreatic cancer. *Lancet*. **2011**, *378* (9791), 607-620. DOI: 10.1016/s0140-6736(10)62307-0
2. Allemani, C.; Matsuda, T.; Di Carlo, V.; Harewood, R.; Matz, M.; Nikšić, M.; Bonaventure, A.; Valkov, M.; Johnson, C. J.; Estève, J.; Ogunbiyi, O. J.; Azevedo, E. S. G.; Chen, W. Q.; Eser, S.; Engholm, G.; Stiller, C. A.; Monnereau, A.; Woods, R. R.; Visser, O.; Lim, G. H.; Aitken, J.; Weir, H. K.; Coleman, M. P. Global surveillance of trends in cancer survival 2000-14 (CONCORD-3): analysis of individual records for 37 513 025 patients diagnosed with one of 18 cancers from 322 population-based registries in 71 countries. *Lancet*. **2018**, *391* (10125), 1023-1075. DOI: 10.1016/s0140-6736(17)33326-3
3. Bray, F.; Ferlay, J.; Soerjomataram, I.; Siegel, R. L.; Torre, L. A.; Jemal, A. Global cancer statistics 2018: GLOBOCAN estimates of incidence and mortality worldwide for 36 cancers in 185 countries. *CA Cancer J. Clin.* **2018**, *68* (6), 394-424. DOI: 10.3322/caac.21492
4. Kamisawa, T.; Wood, L. D.; Itoi, T.; Takaori, K. Pancreatic cancer. *Lancet*. **2016**, *388* (10039), 73-85. DOI: 10.1016/s0140-6736(16)00141-0
5. Labib, P. L.; Goodchild, G.; Pereira, S. P. Molecular Pathogenesis of Cholangiocarcinoma. *BMC Cancer*. **2019**, *19* (1), 185. DOI: 10.1186/s12885-019-5391-0
6. Pereira, S. P.; Oldfield, L.; Ney, A.; Hart, P. A.; Keane, M. G.; Pandol, S. J.; Li, D.; Greenhalf, W.; Jeon, C. Y.; Koay, E. J.; Almario, C. V.; Halloran, C.; Lennon, A. M.; Costello, E. Early detection of pancreatic cancer. *Lancet Gastroenterol. Hepatol.* **2020**, *5* (7), 698-710. DOI: 10.1016/s2468-1253(19)30416-9

7. Rossi, M. L.; Rehman, A. A.; Gondi, C. S. Therapeutic options for the management of pancreatic cancer. *World J. Gastroenterol.* **2014**, *20* (32), 11142-11159. DOI: 10.3748/wjg.v20.i32.11142
8. Neoptolemos, J. P.; Kleeff, J.; Michl, P.; Costello, E.; Greenhalf, W.; Palmer, D. H. Therapeutic developments in pancreatic cancer: current and future perspectives. *Nat. Rev. Gastroenterol. Hepatol.* **2018**, *15* (6), 333-348. DOI: 10.1038/s41575-018-0005-x
9. Mohammad, G. H.; Vassileva, V.; Acedo, P.; Olde Damink, S. W. M.; Malago, M.; Dhar, D. K.; Pereira, S. P. Targeting Pyruvate Kinase M2 and Lactate Dehydrogenase A Is an Effective Combination Strategy for the Treatment of Pancreatic Cancer. *Cancers.* **2019**, *11* (9), DOI: 10.3390/cancers11091372
10. Strobel, O.; Neoptolemos, J.; Jäger, D.; Büchler, M. W. Optimizing the outcomes of pancreatic cancer surgery. *Nat. Rev. Clin. Oncol.* **2019**, *16* (1), 11-26. DOI: 10.1038/s41571-018-0112-1
11. Garcia-Sampedro, A.; Gaggia, G.; Ney, A.; Mahamed, I.; Acedo, P. The State-of-the-Art of Phase II/III Clinical Trials for Targeted Pancreatic Cancer Therapies. *J. Clin. Med.* **2021**, *10* (4), DOI: 10.3390/jcm10040566
12. Han, W.; Chilkoti, A.; Lopez, G. P. Self-assembled hybrid elastin-like polypeptide/silica nanoparticles enable triggered drug release. *Nanoscale.* **2017**, *9* (18), 6178-6186. DOI: 10.1039/c7nr00172j
13. Ryu, J. S.; Raucher, D. Elastin-like polypeptide for improved drug delivery for anticancer therapy: preclinical studies and future applications. *Expert Opin. Drug Deliv.* **2015**, *12* (4), 653-667. DOI: 10.1517/17425247.2015.974546
14. MacEwan, S. R.; Chilkoti, A. Applications of elastin-like polypeptides in drug delivery. *J. Control. Release.* **2014**, *190*, 314-330. DOI: 10.2174/0929867325666180508094637
15. Pina, M. J.; Alex, S. M.; Arias, F. J.; Santos, M.; Rodriguez-Cabello, J. C.; Ramesan, R. M.; Sharma, C. P. Elastin-like recombinamers with acquired functionalities for gene-delivery applications. *J. Biomed. Mater. Res. A.* **2015**, *103* (10), 3166-3178. DOI: 10.1002/jbm.a.35455
16. Arias, F. J.; Santos, M.; Ibanez-Fonseca, A.; Pina, M. J.; Serrano, S. Elastin-Like Recombinamers As Smart Drug Delivery Systems. *Curr. Drug Targets.* **2018**, *19* (4), 360-379. DOI: 10.2174/1389450117666160201114617
17. MacKay, J. A.; Chen, M.; McDaniel, J. R.; Liu, W.; Simnick, A. J.; Chilkoti, A. Self-assembling chimeric polypeptide-doxorubicin conjugate nanoparticles that abolish tumours after a single injection. *Nat. Mater.* **2009**, *8* (12), 993-999. DOI: 10.1038/nmat2569
18. Rodriguez-Cabello, J. C.; Pina, M. J.; Ibanez-Fonseca, A.; Fernandez-Colino, A.; Arias, F. J. Nanotechnological Approaches to Therapeutic Delivery Using Elastin-Like Recombinamers. *Bioconjug. Chem.* **2015**, *26* (7), 1252-1265. DOI: 10.1021/acs.bioconjchem.5b00183
19. Pina, M. J.; Girotti, A.; Santos, M.; Rodriguez-Cabello, J. C.; Arias, F. J. Biocompatible ELR-Based Polyplexes Coated with MUC1 Specific Aptamers and Targeted for Breast Cancer Gene Therapy. *Mol. Pharm.* **2016**, *13* (3), 795-808. DOI: 10.1021/acs.molpharmaceut.5b00712
20. Rodriguez-Cabello, J. C.; Arias, F. J.; Rodrigo, M. A.; Girotti, A. Elastin-like polypeptides in drug delivery. *Adv. Drug Deliv. Rev.* **2016**, *97*, 85-100. DOI: 10.1016/j.addr.2015.12.007
21. Fernandez-Colino, A.; Quinteros, D. A.; Allemandi, D. A.; Girotti, A.; Palma, S. D.; Arias, F. J. Self-Assembling Elastin-Like Hydrogels for Timolol Delivery: Development of an Ophthalmic Formulation Against Glaucoma. *Mol. Pharm.* **2017**, *14* (12), 4498-4508. DOI: 10.1021/acs.molpharmaceut.7b00615
22. Gonzalez-Valdivieso, J.; Borrego, B.; Girotti, A.; Moreno, S.; Brun, A.; Bermejo-Martin, J. F.; Arias, F. J. A DNA Vaccine Delivery Platform Based on Elastin-Like Recombinamer Nanosystems for Rift Valley Fever Virus. *Mol. Pharm.* **2020**, *17* (5), 1608-1620. DOI: 10.1021/acs.molpharmaceut.0c00054
23. Vallejo, R.; Gonzalez-Valdivieso, J.; Santos, M.; Rodriguez-Rojo, S.; Arias, F. J. Production of elastin-like recombinamer-based nanoparticles for docetaxel encapsulation and use as smart

drug-delivery systems using a supercritical anti-solvent process. *J. Ind. Eng. Chem.* **2021**, *93*, 361-374. DOI: 10.1016/j.jiec.2020.10.013

24. Spencer, D. S.; Puranik, A. S.; Peppas, N. A. Intelligent Nanoparticles for Advanced Drug Delivery in Cancer Treatment. *Curr. Opin. Chem. Eng.* **2015**, *7*, 84-92. DOI: 10.1016/j.coche.2014.12.003

25. Di Carlo, C.; Brandi, J.; Cecconi, D. Pancreatic cancer stem cells: Perspectives on potential therapeutic approaches of pancreatic ductal adenocarcinoma. *World J. Stem Cells.* **2018**, *10* (11), 172-182. DOI: 10.4252/wjsc.v10.i11.172

26. Gonzalez-Valdivieso, J.; Girotti, A.; Schneider, J.; Arias, F. J. Advanced nanomedicine and cancer: Challenges and opportunities in clinical translation. *Int. J. Pharm.* **2021**, *599*, 120438-120446. DOI: 10.1016/j.ijpharm.2021.120438

27. Torchilin, V. P. Drug targeting. *Eur. J. Pharm. Sci.* **2000**, *11*, 81-91. DOI: 10.1016/s0928-0987(00)00166-4

28. Quader, S.; Kataoka, K. Nanomaterial-Enabled Cancer Therapy. *Mol. Ther.* **2017**, *25* (7), 1501-1513. DOI: 10.1016/j.yymthe.2017.04.026

29. Matsumura, Y.; Maeda, H. A new concept for macromolecular therapeutics in cancer chemotherapy: mechanism of tumor-tropic accumulation of proteins and the antitumor agent smancs. *Cancer Res.* **1986**, *46* (12), 6387-6392.

30. Jain, R. K. Transport of molecules, particles, and cells in solid tumors. *Annu. Rev. Biomed. Eng.* **1999**, *1*, 241-263. DOI: 10.1146/annurev.bioeng.1.1.241

31. Davis, M. E.; Chen, Z. G.; Shin, D. M. Nanoparticle therapeutics: an emerging treatment modality for cancer. *Nat. Rev. Drug Discov.* **2008**, *7* (9), 771-782. DOI: 10.1038/nrd2614

32. Maeda, H.; Bharate, G. Y.; Daruwalla, J. Polymeric drugs for efficient tumor-targeted drug delivery based on EPR-effect. *Eur. J. Pharm. Biopharm.* **2009**, *71* (3), 409-419. DOI: 10.1016/j.ejpb.2008.11.010

33. Owens, D. E., 3rd; Peppas, N. A. Opsonization, biodistribution, and pharmacokinetics of polymeric nanoparticles. *Int. J. Pharm.* **2006**, *307* (1), 93-102. DOI: 10.1016/j.ijpharm.2005.10.010

34. Byrne, J. D.; Betancourt, T.; Brannon-Peppas, L. Active targeting schemes for nanoparticle systems in cancer therapeutics. *Adv. Drug Deliv. Rev.* **2008**, *60* (15), 1615-1626. DOI: 10.1016/j.addr.2008.08.005

35. Trabulo, S.; Aires, A.; Aicher, A.; Heeschen, C.; Cortajarena, A. L. Multifunctionalized iron oxide nanoparticles for selective targeting of pancreatic cancer cells. *Biochim. Biophys. Acta Gen. Subj.* **2017**, *1861* (6), 1597-1605. DOI: 10.1016/j.bbagen.2017.01.035

36. Luo, J.; Manning, B. D.; Cantley, L. C. Targeting the PI3K-Akt pathway in human cancer: rationale and promise. *Cancer Cell.* **2003**, *4* (4), 257-262. DOI: 10.1016/s1535-6108(03)00248-4

37. Cantley, L. C. The phosphoinositide 3-kinase pathway. *Science.* **2002**, *296* (5573), 1655-1657. DOI: 10.1126/science.296.5573.1655

38. Shariati, M.; Meric-Bernstam, F. Targeting AKT for cancer therapy. *Expert Opin. Investig. Drugs.* **2019**, *28* (11), 977-988. DOI: 10.1080/13543784.2019.1676726

39. Song, M.; Bode, A. M.; Dong, Z.; Lee, M. H. AKT as a Therapeutic Target for Cancer. *Cancer Res.* **2019**, *79* (6), 1019-1031. DOI: 10.1158/0008-5472.can-18-2738

40. Massihnia, D.; Avan, A.; Funel, N.; Maftouh, M.; van Krieken, A.; Granchi, C.; Raktoe, R.; Boggi, U.; Aicher, B.; Minutolo, F.; Russo, A.; Leon, L. G.; Peters, G. J.; Giovannetti, E. Phospho-Akt overexpression is prognostic and can be used to tailor the synergistic interaction of Akt inhibitors with gemcitabine in pancreatic cancer. *J. Hematol. Oncol.* **2017**, *10* (1), 9. DOI: 10.1186/s13045-016-0371-1

41. Bellacosa, A.; Testa, J. R.; Staal, S. P.; Tsichlis, P. N. A retroviral oncogene, akt, encoding a serine-threonine kinase containing an SH2-like region. *Science.* **1991**, *254* (5029), 274-277. doi: 10.1126/science.1833819

42. Hirata, N.; Suizu, F.; Matsuda-Lennikov, M.; Edamura, T.; Bala, J.; Noguchi, M. Inhibition of Akt kinase activity suppresses entry and replication of influenza virus. *Biochem. Biophys. Res. Commun.* **2014**, *450* (1), 891-898. DOI: 10.1016/j.bbrc.2014.06.077
43. Hiromura, M.; Okada, F.; Obata, T.; Auguin, D.; Shibata, T.; Roumestand, C.; Noguchi, M. Inhibition of Akt kinase activity by a peptide spanning the betaA strand of the proto-oncogene TCL1. *J. Biol. Chem.* **2004**, *279* (51), 53407-53418. DOI: 10.1074/jbc.M403775200
44. Rubio-Viqueira, B.; Jimeno, A.; Cusatis, G.; Zhang, X.; Iacobuzio-Donahue, C.; Karikari, C.; Shi, C.; Danenberg, K.; Danenberg, P. V.; Kuramochi, H.; Tanaka, K.; Singh, S.; Salimi-Moosavi, H.; Bouraoud, N.; Amador, M. L.; Altiok, S.; Kulesza, P.; Yeo, C.; Messersmith, W.; Eshleman, J.; Hruban, R. H.; Maitra, A.; Hidalgo, M. An in vivo platform for translational drug development in pancreatic cancer. *Clin. Cancer Res.* **2006**, *12* (15), 4652-4661. DOI: 10.1158/1078-0432.ccr-06-0113
45. Rubio-Viqueira, B.; Hidalgo, M. Direct in vivo xenograft tumor model for predicting chemotherapeutic drug response in cancer patients. *Clin. Pharmacol. Ther.* **2009**, *85* (2), 217-221. DOI: 10.1038/clpt.2008.200
46. Hidalgo, M.; Amant, F.; Biankin, A. V.; Budinska, E.; Byrne, A. T.; Caldas, C.; Clarke, R. B.; de Jong, S.; Jonkers, J.; Maelandsmo, G. M.; Roman-Roman, S.; Seoane, J.; Trusolino, L.; Villanueva, A. Patient-derived xenograft models: an emerging platform for translational cancer research. *Cancer Discov.* **2014**, *4* (9), 998-1013. DOI: 10.1158/2159-8290.cd-14-0001
47. Sia, D.; Moeini, A.; Labгаа, I.; Villanueva, A. The future of patient-derived tumor xenografts in cancer treatment. *Pharmacogenomics.* **2015**, *16* (14), 1671-1683. DOI: 10.2217/pgs.15.102
48. Aparicio, S.; Hidalgo, M.; Kung, A. L. Examining the utility of patient-derived xenograft mouse models. *Nat. Rev. Cancer.* **2015**, *15* (5), 311-316. DOI: 10.1038/nrc3944
49. Gonzalez-Valdivieso, J.; Girotti, A.; Munoz, R.; Rodriguez-Cabello, J. C.; Arias, F. J. Self-Assembling ELR-Based Nanoparticles as Smart Drug-Delivery Systems Modulating Cellular Growth via Akt. *Biomacromolecules.* **2019**, *20* (5), 1996-2007. DOI: 10.1021/acs.biomac.9b00206
50. Courtois, S.; de Luxan-Delgado, B.; Penin-Peyta, L.; Royo-Garcia, A.; Parejo-Alonso, B.; Jagust, P.; Alcalá, S.; Rubiolo, J. A.; Sanchez, L.; Sainz, B.; Heeschen, C.; Sancho, P. Inhibition of Mitochondrial Dynamics Preferentially Targets Pancreatic Cancer Cells with Enhanced Tumorigenic and Invasive Potential. *Cancers.* **2021**, *13* (4), 698. DOI: 10.3390/cancers13040698
51. Rodriguez-Cabello, J. C.; Girotti, A.; Ribeiro, A.; Arias, F. J. Synthesis of genetically engineered protein polymers (recombinamers) as an example of advanced self-assembled smart materials. *Methods Mol Biol.* **2012**, *811*, 17-38. DOI: 10.1007/978-1-61779-388-2\_2
52. Sallach, R. E.; Cui, W.; Balderrama, F.; Martinez, A. W.; Wen, J.; Haller, C. A.; Taylor, J. V.; Wright, E. R.; Long, R. C., Jr.; Chaikof, E. L. Long-term biostability of self-assembling protein polymers in the absence of covalent crosslinking. *Biomaterials.* **2010**, *31* (4), 779-791. DOI: 10.1016/j.biomaterials.2009.09.082
53. Garcia-Arevalo, C.; Bermejo-Martin, J. F.; Rico, L.; Iglesias, V.; Martin, L.; Rodriguez-Cabello, J. C.; Arias, F. J. Immunomodulatory nanoparticles from elastin-like recombinamers: single-molecules for tuberculosis vaccine development. *Mol. Pharm.* **2013**, *10* (2), 586-597. DOI: 10.1021/mp300325v
54. Ohmori, N.; Niidome, T.; Wada, A.; Hirayama, T.; Hatakeyama, T.; Aoyagi, H. The enhancing effect of anionic alpha-helical peptide on cationic peptide-mediated transfection systems. *Biochem. Biophys. Res. Commun.* **1997**, *235* (3), 726-729. DOI: 10.1006/bbrc.1997.6880
55. Kirana, C.; Shi, H.; Laing, E.; Hood, K.; Miller, R.; Bethwaite, P.; Keating, J.; Jordan, T. W.; Hayes, M.; Stubbs, R. Cathepsin D Expression in Colorectal Cancer: From Proteomic Discovery through Validation Using Western Blotting, Immunohistochemistry, and Tissue Microarrays. *Int. J. Proteomics.* **2012**, *2012*, 245819. DOI: 10.1155/2012/245819
56. Bure, C.; Maget, R.; Delmas, A. F.; Pichon, C.; Midoux, P. Histidine-rich peptide: evidence for a single zinc-binding site on H5WYG peptide that promotes membrane fusion at neutral pH. *J. Mass Spectrom.* **2009**, *44* (1), 81-89. DOI: 10.1002/jms.1473

57. Li, Y.; Gu, N. Thermodynamics of charged nanoparticle adsorption on charge-neutral membranes: a simulation study. *J. Phys. Chem. B.* **2010**, *114* (8), 2749-2754. DOI: 10.1021/jp904550b
58. Lin, J.; Zhang, H.; Chen, Z.; Zheng, Y. Penetration of lipid membranes by gold nanoparticles: insights into cellular uptake, cytotoxicity, and their relationship. *ACS Nano.* **2010**, *4* (9), 5421-5429. DOI: 10.1021/nn1010792
59. Malam, Y.; Loizidou, M.; Seifalian, A. M. Liposomes and nanoparticles: nanosized vehicles for drug delivery in cancer. *Trends Pharmacol. Sci.* **2009**, *30* (11), 592-599. DOI: 10.1016/j.tips.2009.08.004
60. Arvizo, R. R.; Miranda, O. R.; Thompson, M. A.; Pabelick, C. M.; Bhattacharya, R.; Robertson, J. D.; Rotello, V. M.; Prakash, Y. S.; Mukherjee, P. Effect of nanoparticle surface charge at the plasma membrane and beyond. *Nano Lett.* **2010**, *10* (7), 2543-2548. DOI: 10.1021/nl101140t
61. Garcia, P. L.; Miller, A. L.; Yoon, K. J. Patient-Derived Xenograft Models of Pancreatic Cancer: Overview and Comparison with Other Types of Models. *Cancers.* **2020**, *12* (5), DOI: 10.3390/cancers12051327
62. Hwang, C. I.; Boj, S. F.; Clevers, H.; Tuveson, D. A. Preclinical models of pancreatic ductal adenocarcinoma. *J. Pathol.* **2016**, *238* (2), 197-204. DOI: 10.1002/path.4651
63. GEPIA. <http://gepia.cancer-pku.cn/index.html> (accessed 2021-05-26).
64. Mantovani, A. Molecular pathways linking inflammation and cancer. *Curr. Mol. Med.* **2010**, *10* (4), 369-373. DOI: 10.2174/156652410791316968
65. Huang, Q.; Zhan, L.; Cao, H.; Li, J.; Lyu, Y.; Guo, X.; Zhang, J.; Ji, L.; Ren, T.; An, J.; Liu, B.; Nie, Y.; Xing, J. Increased mitochondrial fission promotes autophagy and hepatocellular carcinoma cell survival through the ROS-modulated coordinated regulation of the NFKB and TP53 pathways. *Autophagy.* **2016**, *12* (6), 999-1014. DOI: 10.1080/15548627.2016.1166318
66. Porter, A. G.; Janicke, R. U. Emerging roles of caspase-3 in apoptosis. *Cell Death Differ.* **1999**, *6* (2), 99-104. DOI: 10.1038/sj.cdd.4400476
67. Savitskaya, M. A.; Onishchenko, G. E. Mechanisms of Apoptosis. *Biochemistry.* **2015**, *80* (11), 1393-1405. DOI: 10.1134/s0006297915110012
68. Zhao, H. F.; Wang, J.; Tony To, S. S. The phosphatidylinositol 3-kinase/Akt and c-Jun N-terminal kinase signaling in cancer: Alliance or contradiction? (Review). *Int. J. Oncol.* **2015**, *47* (2), 429-436. DOI: 10.3892/ijo.2015.3052
69. Choi, Y.; Ko, Y. S.; Park, J.; Choi, Y.; Kim, Y.; Pyo, J. S.; Jang, B. G.; Hwang, D. H.; Kim, W. H.; Lee, B. L. HER2-induced metastasis is mediated by AKT/JNK/EMT signaling pathway in gastric cancer. *World J. Gastroenterol.* **2016**, *22* (41), 9141-9153. DOI: 10.3748/wjg.v22.i41.9141
70. Raucher, D.; Massodi, I.; Bidwell, G. L. Thermally targeted delivery of chemotherapeutics and anti-cancer peptides by elastin-like polypeptide. *Expert Opin. Drug Deliv.* **2008**, *5* (3), 353-369. DOI: 10.1517/17425247.5.3.353
71. Santos, M.; Serrano-Ducar, S.; Gonzalez-Valdivieso, J.; Vallejo, R.; Girotti, A.; Cuadrado, P.; Arias, F. J. Genetically Engineered Elastin-based Biomaterials for Biomedical Applications. *Curr. Med. Chem.* **2019**, *26* (40), 7117-7146. DOI: 10.2174/0929867325666180508094637
72. Lee, C.; Guo, H.; Klingam, W.; Janga, S. R. Berunda Polypeptides: Biheaded Rapamycin Carriers for Subcutaneous Treatment of Autoimmune Dry Eye Disease. *Mol. Pharm.* **2019**, *16* (7), 3024-3039. DOI: 10.1021/acs.molpharmaceut.9b00263
73. Shi, P.; Aluri, S.; Lin, Y. A.; Shah, M.; Edman, M.; Dhandhukia, J.; Cui, H.; MacKay, J. A. Elastin-based protein polymer nanoparticles carrying drug at both corona and core suppress tumor growth in vivo. *J. Control. Release.* **2013**, *171* (3), 330-338. DOI: 10.1016/j.jconrel.2013.05.013
74. Janib, S. M.; Liu, S.; Park, R.; Pastuszka, M. K.; Shi, P.; Moses, A. S.; Orosco, M. M.; Lin, Y. A.; Cui, H.; Conti, P. S.; Li, Z.; MacKay, J. A. Kinetic quantification of protein polymer nanoparticles using non-invasive imaging. *Integr. Biol.* **2013**, *5* (1), 183-194. DOI: 10.1039/c2ib20169k



75. Hu, J.; Wang, G.; Liu, X.; Gao, W. Enhancing Pharmacokinetics, Tumor Accumulation, and Antitumor Efficacy by Elastin-Like Polypeptide Fusion of Interferon Alpha. *Adv. Mater.* **2015**, *27* (45), 7320-7324. DOI: 10.1002/adma.201503440
76. Jani, P.; Halbert, G. W.; Langridge, J.; Florence, A. T. Nanoparticle uptake by the rat gastrointestinal mucosa: quantitation and particle size dependency. *J. Pharm. Pharmacol.* **1990**, *42* (12), 821-826. DOI: 10.1111/j.2042-7158.1990.tb07033.x
77. Frohlich, E.; Roblegg, E. Models for oral uptake of nanoparticles in consumer products. *Toxicology.* **2012**, *291* (1-3), 10-17. DOI: 10.1016/j.tox.2011.11.004
78. Bergin, I. L.; Witzmann, F. A. Nanoparticle toxicity by the gastrointestinal route: evidence and knowledge gaps. *Int. J. Biomed. Nanosci. Nanotechnol.* **2013**, *3* (1-2), DOI: 10.1504/ijbnn.2013.054515
79. Walczak, A. P.; Kramer, E.; Hendriksen, P. J.; Helsdingen, R.; van der Zande, M.; Rietjens, I. M.; Bouwmeester, H. In vitro gastrointestinal digestion increases the translocation of polystyrene nanoparticles in an in vitro intestinal co-culture model. *Nanotoxicology.* **2015**, *9* (7), 886-894. DOI: 10.3109/17435390.2014.988664
80. Clark, M. A.; Jepson, M. A.; Hirst, B. H. Exploiting M cells for drug and vaccine delivery. *Adv. Drug Deliv. Rev.* **2001**, *50* (1-2), 81-106. DOI: 10.1016/s0169-409x(01)00149-1
81. des Rieux, A.; Ragnarsson, E. G.; Gullberg, E.; Preat, V.; Schneider, Y. J.; Artursson, P. Transport of nanoparticles across an in vitro model of the human intestinal follicle associated epithelium. *Eur. J. Pharm. Sci.* **2005**, *25* (4-5), 455-465. DOI: 10.1016/j.ejps.2005.04.015
82. Crater, J. S.; Carrier, R. L. Barrier properties of gastrointestinal mucus to nanoparticle transport. *Macromol. Biosci.* **2010**, *10* (12), 1473-1483. DOI: 10.1002/mabi.201000137
83. Yang, D.; Liu, D.; Qin, M.; Chen, B.; Song, S.; Dai, W.; Zhang, H.; Wang, X.; Wang, Y.; He, B.; Tang, X.; Zhang, Q. Intestinal Mucin Induces More Endocytosis but Less Transcytosis of Nanoparticles across Enterocytes by Triggering Nanoclustering and Strengthening the Retrograde Pathway. *ACS Appl. Mater. Interfaces.* **2018**, *10* (14), 11443-11456. DOI: 10.1021/acsami.7b19153
84. Shi, J.; Kantoff, P. W.; Wooster, R.; Farokhzad, O. C. Cancer nanomedicine: progress, challenges and opportunities. *Nat. Rev. Cancer.* **2017**, *17* (1), 20-37. DOI: 10.1038/nrc.2016.108
85. Jain, R. K. Transport of molecules in the tumor interstitium: a review. *Cancer Res.* **1987**, *47* (12), 3039-3051.
86. Behzadi, S.; Serpooshan, V.; Tao, W.; Hamaly, M. A.; Alkawareek, M. Y.; Dreaden, E. C.; Brown, D.; Alkilany, A. M.; Farokhzad, O. C.; Mahmoudi, M. Cellular uptake of nanoparticles: journey inside the cell. *Chem. Soc. Rev.* **2017**, *46* (14), 4218-4244. DOI: 10.1039/c6cs00636a
87. Kleiner, D. E.; Brunt, E. M.; Van Natta, M.; Behling, C.; Contos, M. J.; Cummings, O. W.; Ferrell, L. D.; Liu, Y. C.; Torbenson, M. S.; Unalp-Arida, A.; Yeh, M.; McCullough, A. J.; Sanyal, A. J. Design and validation of a histological scoring system for nonalcoholic fatty liver disease. *Hepatology.* **2005**, *41* (6), 1313-1321. DOI: 10.1002/hep.20701
88. Gibson-Corley, K. N.; Olivier, A. K.; Meyerholz, D. K. Principles for valid histopathologic scoring in research. *Vet. Pathol.* **2013**, *50* (6), 1007-1015. DOI: 10.1177/0300985813485099
89. Sachdeva, J.; Dai, W.; Kloner, R. A. Functional and histological assessment of an experimental model of Takotsubo's cardiomyopathy. *J. Am. Heart Assoc.* **2014**, *3* (3), e000921. DOI: 10.1161/jaha.114.000921